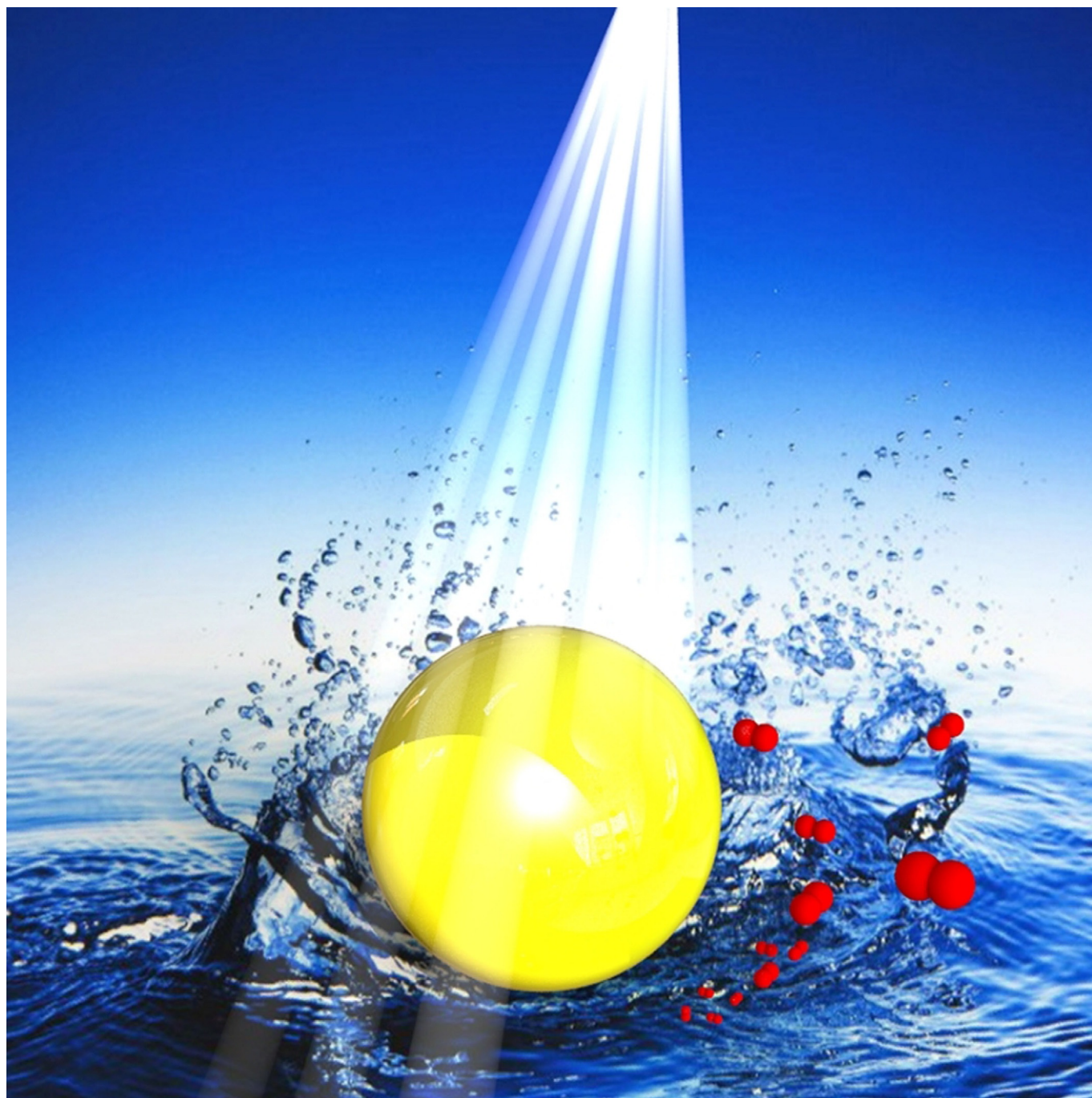


Special  
Issue

# Strategies for Plasmonic Hot-Electron-Driven Photoelectrochemical Water Splitting

Turkan Gamze Ulusoy Ghobadi,<sup>[a, b, c]</sup> Amir Ghobadi,<sup>[d, e]</sup> Ekmel Ozbay,<sup>\*[a, d, e, f]</sup> and Ferdi Karadas<sup>\*[a, g]</sup>



Photoelectrochemical water splitting (PEC-WS) was inspired by the natural photosynthesis process that utilizes sunlight energy to produce chemical energy through splitting water to form hydrogen and oxygen. One recent promising and innovative approach in this field is to implement the concept of plasmonic to PEC-WS devices. This Review provides a systematic overview of the plasmonic and hot-electron-driven PEC-WS and elucidates their possible mechanisms for plasmon-mediated energy transfer. In the first section, we provide a brief summary of the basics of PEC-WS and the strategies employed to maximize its conversion efficiency. Highlighting the advantages of the plasmonic-based PEC system, in the next part we cluster

our discussion based on the basics of plasmonics and the involved energy transfer mechanisms, which are classified as radiative (scattering, optical near field coupling) and nonradiative energy transfer (hot electron injection, plasmon resonant energy transfer) processes for plasmonic metal–semiconductor junctions as a photoactive material. Then, the recent research efforts in this field are categorized and discussed in three main sections: 1) nanoplasmonic units, 2) nanostructured support scaffolds, and 3) interface engineering with state-of-the-art demonstrations. Finally, we conclude our Review with pointing out the challenges and perspectives of the plasmonic-based architectures for future water-splitting devices.

## 1. Introduction

The biological systems that drive photosynthesis have been under vigorous research in the recent years since it is considered to be the key process for the sustainability of life. Photosynthesis could simply be described as the conversion of sunlight to chemical energy where water is activated by sunlight to produce high-energy chemicals. Although many enzymes with different functionalities are involved in this process, it is known to constitute three essential steps: (i) an antenna system for light harvesting; (ii) a donor-acceptor system for charge separation; and (iii) catalytic sites for water oxidation and water reduction. In natural photosynthesis, the water oxidation active sites are attached to protein chains in a specific configuration to release oxygen and protons in each catalytic cycle.<sup>[1]</sup> In this system, the sunlight is harvested by an “antenna” system that is made of molecular pigments (chlorophyll, carotenoids, phycobilins, and etc.). The main function of the

antenna system is to transfer the absorbed energy to their respective reaction centers through a transport layer (i.e., the donor-acceptor system). The acceptor part is connected to the active sites of water oxidation, which are bonded to protein chains. In fact, four manganese atoms, which are surrounded by 2500 pigments, are required to produce oxygen from water. Therefore, the efficiency of natural photosynthesis is governed by the densities and portions of these pigments and catalytic sites.<sup>[2]</sup> The complex nature of this process also implies that challenging processes such as light-driven water oxidation can be achieved with a set of well-designed materials, which are equipped to handle specific parts of the process.

The concept of photoelectrochemical water splitting (PEC-WS) has emerged simply as a result of an effort to mimic photosynthesis by coupling solar energy and electrochemical water splitting in a single device.<sup>[3,4]</sup> Although this approach provides a big step forward towards the conversion of solar energy to chemical energy by applying a small to no external bias, the necessity of using a combination of materials, as in the case of natural photosynthesis, makes the design of an ideal device rather challenging.<sup>[5]</sup> Nevertheless, the recently growing interest on PEC systems led to more than 3,000 scientific papers and several books in the last 5 years. While each of the previously studied systems mainly differs in the type of materials used, they adopt the same principle. It is then evident that the right combination of materials, serving as an antenna, donor-acceptor, and catalyst, must be used in a proper fashion to construct a PEC-WS cell and thus the selection of an ideal material for a specific task should be made also based on the properties of the other material components of the device. Therefore, the understanding of the overall mechanism is of critical importance to introduce new materials and methodologies to the field. There are already several comprehensive reviews in the literature and the reader is encouraged to refer to them for a detailed discussion on photoelectrochemical water splitting recent strategies, cell designs, and materials used for this purpose.<sup>[4,6–16]</sup> Herein, a short introduction on the basic working principle of PEC-WS devices and common materials will be given only to explain why the concept of “Hot-Electron and Plasmonic Driven Photoelectrochemical Water Splitting” has a promising potential and how it can contribute to the field. The next chapters are devoted to the basic operation of

[a] T. G. U. Ghobadi, Prof. E. Ozbay, Assist. Prof. F. Karadas  
UNAM-National Nanotechnology Research Center  
Bilkent University, Ankara 06800 (Turkey)  
E-mail: ozbay@bilkent.edu.tr  
karadas@fen.bilkent.edu.tr

[b] T. G. U. Ghobadi  
Institute of Materials Science and Nanotechnology  
Bilkent University, Ankara 06800 (Turkey)

[c] T. G. U. Ghobadi  
Department of Energy Engineering, Faculty of Engineering  
Ankara University, Ankara 06830 (Turkey)

[d] A. Ghobadi, Prof. E. Ozbay  
NANOTAM- Nanotechnology Research Center  
Bilkent University, Ankara 06800 (Turkey)

[e] A. Ghobadi, Prof. E. Ozbay  
Department of Electrical and Electronics Engineering  
Bilkent University, Ankara 06800 (Turkey)

[f] Prof. E. Ozbay  
Department of Physics  
Bilkent University, Ankara 06800 (Turkey)

[g] Assist. Prof. F. Karadas  
Department of Chemistry  
Bilkent University, Ankara 06800 (Turkey)

 The ORCID identification number(s) for the author(s) of this article can be found under: <https://doi.org/10.1002/cptc.201700165>.

 An invited contribution to a Special Issue on Artificial Photosynthesis.

a plasmonic system and recent strategies used to implement this methodology to PEC-WS devices.

## 1.1. Basic Concepts of Photoelectrochemical Water Splitting (PEC-WS)

### 1.1.1. Working Principle

A simple design of a PEC-WS system, which was initially presented in 1972, is shown in Figure 1.<sup>[17]</sup> The basic cell is composed of at least one semiconductor as a photoactive material or photoelectrode and a metal counter electrode that are immersed in an electrolyte and connected by external electric wire. Overall, PEC-WS consists of two half reactions;<sup>[18,19]</sup> i) oxidation of water to oxygen gas ( $O_2$ ) and ii) reduction of protons to hydrogen gas ( $H_2$ ), which take place at the (photo)anode and (photo)cathode, respectively. Generally, the photoanode is

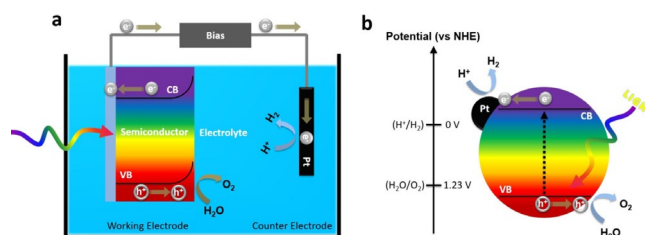


**Figure 1.** Schematic of a) a basic PEC-WS cell including an n-type semiconductor photoanode and a metal cathode that are immersed in an electrolyte and connected by an external electric wire, and the b) particulate form of the photocatalyst.

an n-type semiconductor and photocathode is a p-type semiconductor. Water splitting is thermodynamically an uphill reaction and requires relatively high energy ( $237 \text{ kJ mol}^{-1}$ ),<sup>[20]</sup> which corresponds to a band gap of 1.23 V per electron.

Turkan Gamze Ulusoy Ghobadi received her BS degree in Chemical Engineering from Ankara University, Turkey in 2012. She joined the National Nanotechnology Research Center (UNAM), Institute of Materials Science and Nanotechnology, Bilkent University, Turkey and obtained MS degree in 2015. Currently, she is pursuing her PhD degree in the same department under the guidance of Asst. Prof. Ferdi Karadas from the Chemistry Dept. She became a research assistant in the Dept. of Energy Engineering at Ankara University in 2017. Her current research interests focus on the development of (photo)electrochemical materials for energy storage and conversion systems.



Prof. Dr. Ekmel Ozbay received M.S. and Ph.D. degrees from Stanford University in electrical engineering, in 1989 and 1992. He worked as a post-doctoral research associate at Stanford University and he worked as a scientist in Iowa State University. He joined Bilkent University (Ankara, Turkey) in 1995, where he is currently a full professor in the Physics Department and EEE Department. In 2003, he founded the Bilkent University Nanotechnology Research Center (NANOTAM) where he leads a research group working on nanophotonics, nanometamaterials, nanoelectronics, GaN/AlGaIn MOCVD growth, and GaN based devices. He is the 1997 recipient of the Adolph Lomb Medal of OSA and 2005 European Union Descartes Science award. He worked as an editor for Nature Scientific Reports, Optics Letters, PNFA, and IEEE JQE journals. He has published 420+ articles in SCI journals, including a Science paper on plasmonics. His papers have received 19,000+ SCI citations with an SCI h-index of 70. He has given 145+ invited talks at international conferences. He recently became the CEO of a spin-off company: AB-MicroNano Inc.



Amir Ghobadi received his BS degree in electrical engineering from the University of Tehran, Iran, in 2012. He received his MS degree from the same department at Bilkent University in 2014. Currently, he is working toward his PhD under the supervision of Prof Ekmel Ozbay at Bilkent University. His research involves the design, synthesis, and characterization of novel semiconductor-based optic and photonic devices.



Asst. Prof. Ferdi Karadas received his PhD in molecular magnetism and inorganic coordination compounds in 2009 from Texas A&M University in Texas, USA, under the supervision of Prof. Kim R. Dunbar. Since 2013, he has been a professor in the Department of Chemistry, Bilkent University, Turkey. His research is focused on the development of new materials and molecular hybrid systems for water oxidation and reduction electrocatalysis and dye-sensitized photoelectrocatalytic systems.

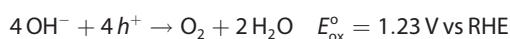


In fact, OER requires to multiple electron transfer during the formation of an O–O bond.<sup>[18,21]</sup> The redox reactions on each electrode occurs by the following mechanisms and standard redox potentials [Eq. (1)]:

Photon Absorption :



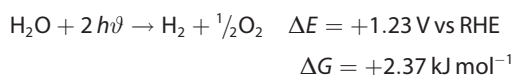
PhotoAnode/Basic :



Cathode/Basic :



Overall :



Before introducing the materials for PEC-WS, it is beneficial to get an idea about how solar energy is converted to chemical energy by means of several kinetic-based processes inside the cell. In PEC-WS, the theory of operation consists of four main steps (Figure 3a);<sup>[22]</sup> 1) light absorption, 2) charge separation, 3) charge collection and 4) catalytic reactions. The first step is mainly dependent on the optical properties of the photoelectrode while the rest are strongly affected by the electronic properties of the photoactive components.

#### 1.1.1.1. Light Absorption and Charge Carrier Photoexcitation

A photoabsorber is mainly a semiconductor with suitable valence band (VB) and conduction band (CB), where the energy difference between these two levels is called the band gap ( $E_g$ ) of the semiconductor. While the bottom energy level of the CB (LUMOs) is a measure of the reducing potential of photoelectrons, the uppermost level of VB (HOMOs) corresponds to the oxidizing potential of photoholes.<sup>[23]</sup> Upon light irradiation, a photon with energy higher than the band gap of the photoabsorber generates electron and hole pairs.<sup>[24]</sup> Since the main requirement of an ideal water splitting system (photoelectrolysis) is the use of only sunlight as a source of energy, a photoelectrode should have strong absorption across the solar spectrum and concurrently its band gap should be higher than the electrochemical water splitting potential of 1.23 V in order to obtain a large amount of photo-excited carriers capable of performing the desired reactions.<sup>[25]</sup> Most of the materials, however, do not meet this energetic requirement.<sup>[4]</sup> Furthermore the theoretical minimum band gap of the photoelectrode needs to be higher than sum of this minimum required potential (1.23 V) and the cathodic and anodic overpotentials (around 100 mV and 300 mV for a current density of  $10 \text{ mA cm}^{-2}$  for catalytic reactions, respectively) which are due to catalyst activation, Ohmic contact losses, and mass transport limitations.<sup>[26,27]</sup> Therefore, the generally accepted minimum optical band gap of a semiconductor should be about 1.6–2.0 eV. Additionally, a certain amount of external bias is, also required for driving electron/hole transfer processes in an overall water splitting device. It should also be noted that recent studies

have proven the operation of an unassisted efficient PEC-WS cell where the PEC system is monolithically integrated to a photovoltaic (PV) cell. In such a system, the external bias is supplied with the PV cell to device for water splitting reactions.<sup>[28,29]</sup>

#### 1.1.1.2. Separation of Photogenerated Charge Carriers

When a photosensitizer is excited, electrons will be excited from VB to CB and holes will be left free at the VB. A portion of these excited carriers will recombine on the semiconductor surface or in the bulk within a few picoseconds (ps) and release their energy in the form of heat or phonons. Thus, rapid separation and collection of photo-induced carriers are desirable to reduce the  $e^-h^+$  recombination and to increase the overall yield of water splitting.<sup>[30]</sup>

During photoelectrocatalysis, a space charge depletion layer occurs at the semiconductor-liquid electrolyte interface (also known solid-liquid junction), which stimulates the upward band bending in a photoanode and downward band bending in a photocathode.<sup>[8,31]</sup> This potential profile, which depends on the relative alignment of the semiconductor work function and the reaction potential, enables the efficient separation of photoinduced charges and prevents the recombination of  $e^-h^+$  pairs.<sup>[32]</sup> Thus, it is favorable to use n-type and p-type semiconductors as photoanode and photocathode candidates, respectively.

#### 1.1.1.3. Collection and Transportation of Charges to Electrode Surfaces

In this step, holes migrate to semiconductor-liquid junction at the n-type photoanode surface (they can also travel to the co-catalyst surface and then to its electrolyte interface) where the oxygen evolution reaction (OER) takes place while electrons reach the counter electrode through an external wire to trigger the hydrogen evolution reaction (HER) at the surface.<sup>[33]</sup> In the case of a photocathode, which is a p-type semiconductor, the photo-activated electrons are transferred to the semiconductor surface and the HER takes place with the mediation of a co-catalyst. Consequently, the OER occurs in the counter electrode material while electrons travel to the photocathode within external bias to recombine with the free holes in the photocathode.

#### 1.1.1.4. Catalytic Reactions at the Surfaces

After the efficient separation of the carriers, these photogenerated electrons and holes are adsorbed on surface active sites to reduce and oxidize water to produce  $\text{H}_2$  and  $\text{O}_2$  gases, respectively. Holes have lower mobility and hence shorter diffusion lengths compared to electrons. Therefore, electrocatalysts can be employed as co-catalysts to enhance the kinetics of the water splitting process by reducing the activation energy for gas evolution.<sup>[34,35]</sup> This method, however, can be applied at the expense of an additional charge transfer resistance as a result of an additional interface introduced to the system. The

oxygen evolution step (photo-oxidation) is the rate-determining step due to its slow kinetics.

The comparison of all the reported systems in the literature is not an easy task because of the rapid growth of the field, substantially various PEC cell designs, and different efficiency parameters reported at different experimental conditions. Nevertheless, the studies indicate that the photoelectrode (both surface and its bulk) are vitally important since the light absorption, charge separation and collection, and catalytic reactions all occur in the same electrode. Thus, improving the optical and electrical characteristics of the photoelectrode material together with its stability is of great importance in this field. This improvement can be attained with novel design architectures and/or the introduction of new materials. In the next section, a brief review on common strategies is conducted in this area.

### 1.1.2. Materials for PEC-WS

Given that most of the solar irradiation energy is concentrated in visible (Vis) and near infrared (NIR) regimes, one of the most prominent features of an optimum light absorber is to have a low band gap ( $E_g < 3$  eV). There are, however, a couple of bottlenecks that make this requirement difficult to satisfy, one of which, as noted hereinabove, is the difference between the energetic location of HER and OER process that are located at 0 V (vs. RHE) and 1.23 V (vs. RHE), respectively. Therefore, the realization of both reactions with a single semiconductor ideally requires an optical band gap larger than 1.23 eV. This value rises up to approx. 1.6 eV for practical applications, which corresponds to a wavelength of  $\approx 774$  nm, due to ohmic losses in different parts of the system. In addition to this requirement, CB energy level of photoanode should lie above the  $H^+/H_2$  (0 V vs. RHE) and VB should be below  $O_2/H_2O$  (1.23 V vs. RHE) under standard conditions. In other words, both the reduction and oxidation potentials of water should be within the band gap of the semiconductor.

Figure 2 shows how well the commonly studied semiconductors satisfy these requirements. The energy difference between the VB and the potential for water oxidation ( $E_{VB}-E_{OER}$ ) is plotted with respect to the energy difference between the CB of the semiconductor and the potential for hydrogen evolution ( $E_{CB}-E_{HER}$ ).<sup>[23,36,37]</sup> Additional potentials (overpotentials) of 200 mV and 400 mV are also considered for HER and OER, respectively, to account for the losses during electrocatalytic processes.<sup>[38,39]</sup> According to the figure, a semiconductor that lies on the right side of the black dashed line has a suitable VB position for water oxidation. The same analogy can be made for water reduction as well. The diagram also displays the comparison of the band gaps of semiconductors in the units of wavelength to show whether the semiconductor is suitable to harvest visible light or not. Therefore, an ideal semiconductor, which can efficiently harvest visible light and derive both water oxidation and reduction, should lie in the highlighted triangular region. For example,  $TiO_2$ , which is considered to be the first example of the photoelectrocatalytic splitting of water, has a suitable VB for water oxidation while it is a poor

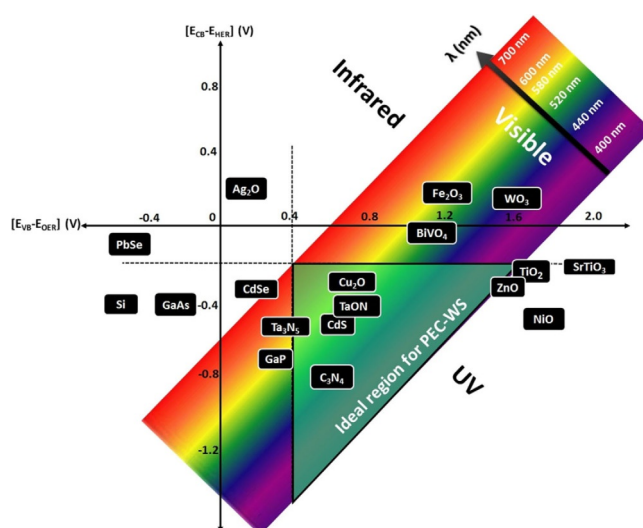


**Figure 2.** Comparison of different semiconductors, in contact with the aqueous electrolyte at pH 0, according to their band gaps (in units of nm) and band positions with respect to HER and OER half-reactions. An additional overpotential of 200 and 400 mV was considered to define the optimum region. Since these overpotentials are merely estimated values (lower overpotentials are available in the literature)<sup>[63,64]</sup> the highlighted region does not retain exact borders.

absorbing semiconductor in the visible region. While  $TiO_2$  remains to be the most studied semiconductor in this field,<sup>[40]</sup> many other  $d^0$  metal oxides, including  $ZrO_2$ ,  $NbO_2$ , and  $WO_3$ ,<sup>[41]</sup>  $d^{10}$  metal oxides involving  $ZnO$ ,<sup>[42]</sup> and even mixed oxides containing both  $d^0$  and  $d^{10}$  metal ions such as  $BiVO_4$ <sup>[43]</sup> have been widely studied. Some of these metal oxides have smaller band gaps than desired and most of them have exhibit poor optical and electrical performances. Moreover, as it can be clearly seen from Figure 2, their band positions are not suitable for performing the whole water splitting reaction. In the case of  $d^{10}$  metal oxides, they are generally more advantageous as photoactive materials in terms of the mobility of photogenerated electrons in the CB and photocatalytic activity due to hybridized empty sp orbitals of typical metals.<sup>[44]</sup> Besides, these large band gap metal oxides, at the other end of the scale, there are several narrow band gap visible light responsive non-oxide semiconductors that can absorb most of the solar irradiation. These materials, however, have the chemical instability deficiency that mitigates their long-term sustainabilities under a high oxidative environment.<sup>[14]</sup> For example, metal chalcogenides, including CdS, appear to be one of the most suitable photocatalysts for overall water splitting, exhibiting band gap energies sufficiently small to allow for the absorption of visible light and having conduction and valence bands at potentials appropriate for water reduction and oxidation (see Figure 2). These metal chalcogenides, however, are not suitable for water oxidation since sulfide and selenide anions are more susceptible to oxidation than water, which causes CdS or CdSe catalysts themselves to be oxidized and degraded over time.<sup>[45]</sup> Therefore, the ideal approach would be the enhancement of optical properties and stabilities of oxide based semiconductors with novel strategies. In recent years, a major part of the

current research revolves around manipulating the band positions and band gaps of already studied semiconductors by doping. Doping could be performed with metal ions and/or non-metal elements since the position of valence and conduction bands are generally according to the type of metal and non-metal ions, respectively.<sup>[46]</sup> A well-known example to this approach is the gradual increase in the valence band energy of a  $d^0$  metal oxide, such as  $Ta_2O_5$ , with increasing the amount of N-doping while the energy of the conduction band remains constant leading to a decrease in the band gap. This method yields a semiconductor, named TaON, which has ideal band positions for overall water splitting (Figure 2).<sup>[47–49]</sup> Another viable method is the incorporation of alkali metal ions to the crystal structure of semiconductors, which has been employed particularly to enhance the stability of the crystal structure and even for the construction of new crystal structures. For example, a study performed on a series of alkali metal tantalates,  $MTaO_3$  ( $M = Li, Na, \text{ and } K$ ), revealed that Ta-O-Ta angle in the crystal structure can be varied by changing the alkali metal ion, which has a direct effect on the band diagram.<sup>[50]</sup>

With decades of investigations since the seminal work in 1972, there is still no semiconductor that simultaneously satisfies all of the requirements mentioned above. Therefore, it is common to combine multiple semiconductors together (building junctions), which is essentially analogous to natural photosynthesis that uses a series of enzymes and molecules that are equipped with specific features. An efficient heterojunction system generally consists of two semiconductors, one of which has a valence band suitable for water oxidation (higher than 1.23 V vs. NHE) while the other one has a conduction band properly suited for water reduction (lower than 0 V vs. NHE). Furthermore, they should have matched band positions with respect to each other to allow for efficient charge separation. For example, an enhancement in the photocurrent density has been achieved with  $BiVO_4-WO_3$ ,<sup>[51,52]</sup>  $TiO_2-WO_3$ ,<sup>[53]</sup>  $TiO_2-SrTiO_3$ ,<sup>[54]</sup>  $BaTiO_3-TiO_2$ ,<sup>[55]</sup>  $ZnO-TiO_2$ ,<sup>[56]</sup> and  $BiVO_4-TiO_2$ <sup>[57]</sup> compared to their single component cases. This methodology has been used for non-oxide semiconductors as well.<sup>[58,59]</sup> The efficiency of the visible absorption can also be improved by coupling the semiconductor with a molecular chromophore (dye-sensitizing). This is known as dye-sensitized photoelectrochemical cells (DSPECs), which consist of a metal oxide coupled to a molecular dye and catalyst assembly (dyad).<sup>[60,61]</sup> As illustrated in the Figure 3a, in the DSPEC system, the absorption of the light is provided using a visible responsive dye. Although promising studies have been introduced by Sun et al. and others, these systems generally suffer from the high tendency of molecular dyads to decompose during the catalytic process.<sup>[62]</sup> Therefore, stability is still the main issue that limits the long-term operation and large scale compatibility of these systems.

In summary, several different strategies<sup>[46]</sup> such as the doping of external elements to tune the band structure, construction of heterojunctions to suppress the recombination of electron-hole pairs, decreasing the particle sizes of the photocatalysts to reduce the migration distance of charge carriers, optimizing the crystal structure to expose more active facets,<sup>[22]</sup> using efficient electrocatalysts for HER and OER, and

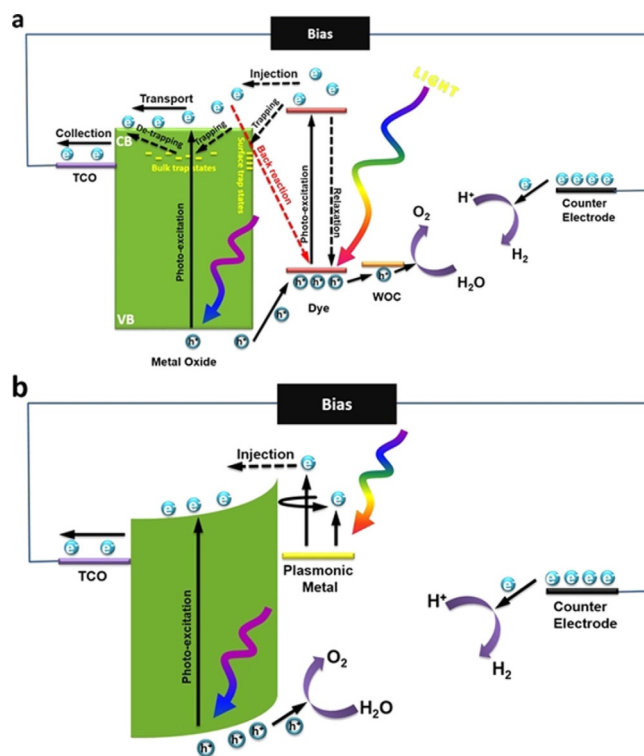


**Figure 3.** The steps involved in the operation of a a) dye sensitized PEC (DSPEC) and b) plasmonic hot-electron-driven PEC systems. In the DSPEC cell, the sensitizer photoactive material is a visible absorptive dye layer while this material is replaced with plasmonic metal NPs in the case of the hot-electron-driven system.

sensitizing the semiconductor with molecular organic or inorganic molecular chromophores have been employed to improve the overall performance of PEC-WS. There are many great reviews related to their performances, limitations, and potentials by analyzing the pathway of energy capture and conversion mechanism in water splitting systems. Among all of the proposed methodologies, the integration of plasmonic metals (mostly noble metals including Au and Ag) with photocatalysts have recently been introduced and it is considered as an effective route to attain high performance and stable water splitting cell.

Comparing with DSPEC system, a plasmonic enhanced water splitting device utilizes the hot electrons inside the metal to drive the HER process. In the other word, in this Scheme, the plasmonic metal acts as the sensitizer layer. This has been schematically shown in Figure 3b. In the next section, we aim to provide an overview of recent strategies toward the development of hot-electron driven photoelectrode designs through optimized parameters for PEC-WS.

## 2. Plasmonics

Since the discovery of the PEC-WS by Honda and Fujishima in 1972, a substantial number of articles (> 3,000 source: Web of Science) have been published in this field. Figure 4 describes the advances in this technology, which started with  $TiO_2$  as a photoanode, followed by heterojunction designs in 1990s and

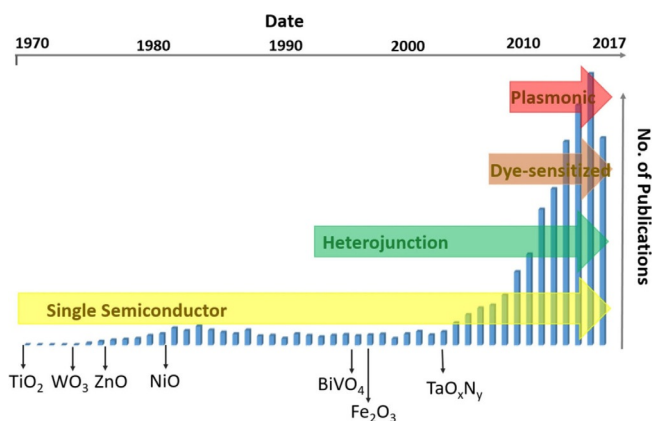


Figure 4. Timeline of emerged technologies in PEC-WS applications.

DSPEC designs applied in PEC-WS systems in 2010s.<sup>[17,65–70]</sup> Although the light absorption enhancement through plasmon resonance in the near surface of the metal emerged in 1960s, usage in light driven water splitting has started for not even after a decade.

## 2.1. Localized Surface Plasmon Resonance

Upon excitation with a frequency close to the natural oscillation frequency, sub-wavelength<sup>[71]</sup> nanosized geometries of noble metal (e.g. Au and Ag) nanoparticles (NPs) can excite localized surface plasmon resonance (LSPR) originated from collective oscillations of the free electrons at the interface of metal-dielectric.<sup>[71–73]</sup> Under this condition, intense localized electric field enhancement can be probed at the NP surface.<sup>[74–77]</sup> LSPR can decay through two main pathways; 1) radiatively or 2) nonradiatively<sup>[78,79]</sup> (see Figure 5). The radiative decay emits photons and transfers the radiated energy isotropically into the surrounding environment. The nonradiative decay of LSPR, however, can generate hot carriers. These hot electrons/holes are formed during the nonradiative relaxation process primarily through electron-electron scattering, which results in intra- and inter-band excitation of the conduction band electrons. The nonradiative decay pertains to the formation of hot-carriers and then these carriers can transfer to a neighboring semiconductor with a proper band alignment. The injection of these carriers to the semiconductor is called internal photoemission and can happen irrespective of the excitation of a plasmon. In this section, we will provide a detailed analysis on the origin and principle of each of these energy transfer mechanisms.

## 2.2. Mechanisms for Plasmon-Mediated Energy Transfer

Upon exciting the LSPR in plasmonic unit, it decays and transfers its energy to the adjacent components through two main processes; 1) radiative or 2) nonradiative energy transfer.<sup>[79]</sup> Based on the geometry of the design including its size, shape, and composition and the nature of its junction with the neighborhood semiconductor, one or some of these mechanisms dominate the functionality of the design. In this section, we

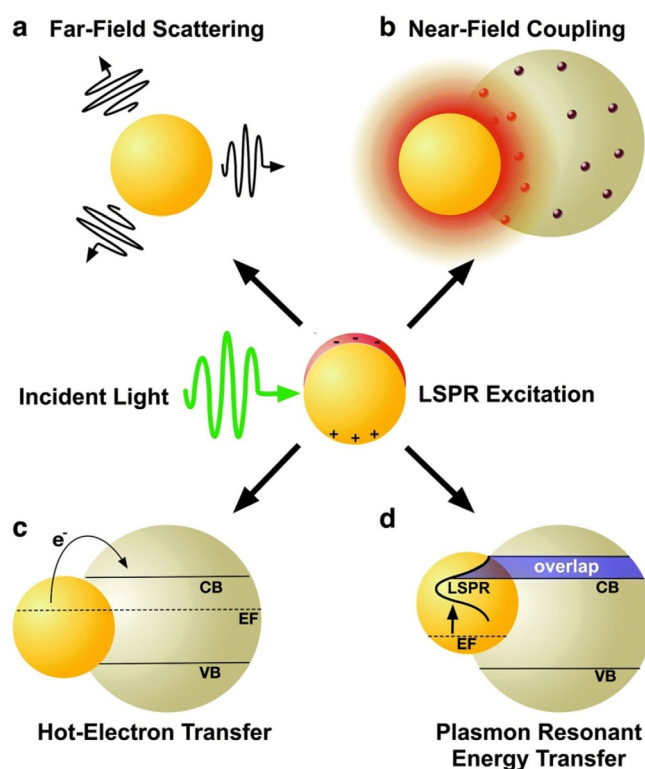


Figure 5. The excitation of localized surface plasmon resonance and different energy transfer mechanisms responsible for plasmon-driven performance enhancement. These mechanisms can be divided into two main parts; radiative and nonradiative. In the radiative process, the energy can be transferred to an adjacent semiconductor through a) far-field scattering or b) near-field coupling. In the nonradiative case, the energy transfer can be obtained by means of c) hot-electron transfer or d) plasmon resonant energy transfer. Reproduced with permission from Ref. [78]. Copyright 2016, The Royal Society of Chemistry.

will render the requirements for the occurrence of each of these mechanisms.

### 2.2.1. Radiative Energy Transfer

In this type of energy transfer, the particle acts as a plasmonic antenna, in which the LSPR relaxes radiatively and transfer its energy by emission of a photon. Taking the antenna terminology into consideration, this power can be decomposed into two main parts; 1) far field propagating of electromagnetic (EM) wave and 2) near field coupling of evanescent modes. Considering the fact that, in the far field propagation, this nanoplasmonic geometry gets activated upon excitation and radiates its energy as a secondary source, this process is called light scattering. While the near field light confinement is named as optical coupling it is responsible for absorption enhancement in the metal-semiconductor nanocomposite. Both of these energy transfers mainly work as a secondary source providing light absorption for the adjacent environment. In other words, these phenomena are not directly responsible for photocurrent enhancement but provide a condition, in which photoactive material generates more electron and hole carriers. In this sec-

tion, details of each of these energy transfer processes will be scrutinized.

### 2.2.1.1. Scattering

As mentioned earlier, if a sub-wavelength particle is illuminated by incident light, its electrons begin to oscillate, which makes a secondary radiation called scattering. If the particle transfers the energy of the exciting light to another energy type, for example, heat, the light is said to be absorbed. In general, to evaluate the absorption or scattering capacity of a system, a term called cross-section with a unit of  $\text{m}^2$  is used. The scattering cross-section is calculated by dividing the integrated total scattered power by the intensity of the light. This property is greatly influenced by the size of plasmonic particle. In dimensions much smaller than the incident wavelength, scattering and absorption cross-sections can be calculated using the following formula [Eqs. (2)–(3)].<sup>[78,80]</sup>

$$\sigma_{\text{abs}} \approx \sigma_{\text{ext}} = k \operatorname{Im}(\alpha) = 4\pi k R^3 \operatorname{Im} \left( \frac{\epsilon_p - \epsilon_m}{\epsilon_p + 2\epsilon_m} \right) \quad (2)$$

$$\sigma_{\text{sca}} = \frac{k^4}{6\pi} |\alpha|^2 = \frac{8\pi}{3} k^4 R^6 \left| \frac{\epsilon_p - \epsilon_m}{\epsilon_p + 2\epsilon_m} \right|^2 \quad (3)$$

where  $k$  is wavenumber,  $R$  is the particle radius,  $\epsilon_m$  is the complex permittivity value of the system, and  $\epsilon_0$  is the surrounding environment permittivity. As this formula implies, the scattering cross-section is proportional to  $R^6$ , while this dependence proportionality is  $R^3$  for absorption case. A better qualitative comparison has been provided in Figure 6a.<sup>[78]</sup> As this figure depicts, the scattering property of the nanosphere is almost negligible compared to that of its absorption cross-section in diameters smaller than 50 nm ( $R < 25$  nm). Therefore, in a plasmonic NP, the absorption is the dominant process affecting the overall optical performance of the system. When the NP diameter exceeds 100 nm, the scattering dominates the absorption cross-section and, therefore, this far field radiation is mainly the property of bigger particles. Moreover, comparing the scattering cross-section with the real cross sectional area of the particle, it can be understood that, at the surface plasmon resonance, the scattering cross section exceeds the geometrical cross section of the NPs.<sup>[81]</sup> For instance, Ag NPs in air have scattering cross-sections that are about an order of magnitude larger than their cross sectional areas at the vicinity of the resonant frequency. That is why a partial coating of plasmonic NPs on a surface with a filling factor much smaller than one can ensure the scattering of the whole incoming light.<sup>[80,81]</sup> It should be noted that scattering is not only a metal NP characteristic but dielectric particles can also scatter the light. Figure 6b compares the scattering and absorption spectra of different sized gold NPs with polystyrene dielectric particle.<sup>[82]</sup> As it can be clearly seen from this panel, a dielectric particle has a scattering property that exponentially decays as we go to larger particle sizes. In fact, when the incident light wavelength is bigger than the particle size it does not see it. However, this

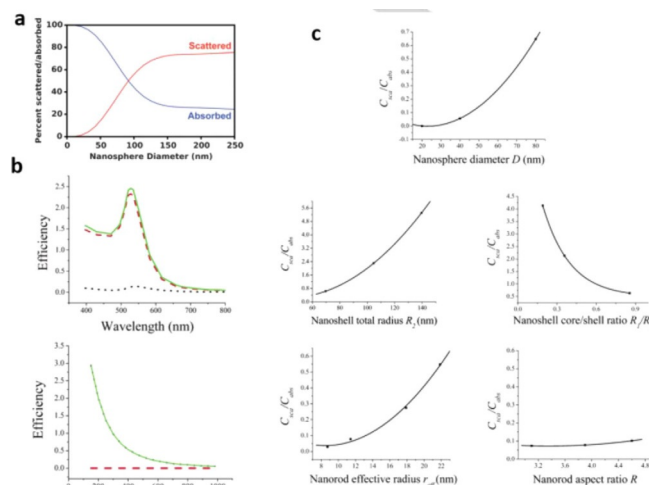


**Figure 6.** a) The scattering and absorption property of a nanosphere as a function of its diameter (reproduced with permission from Ref. [78], copyright 2016, The Royal Society of Chemistry), b) comparing the scattering spectra of metal and dielectric NPs (reproduced with permission from Ref. [82], copyright 2006, American Chemical Society), and c) the ratios between scattering and absorption as a function of plasmonic design shape, size, and composition. (Reproduced with permission from Ref. [82]. Copyright 2006, American Chemical Society).

property does not follow the same trend in the case of metallic Au NPs. This is due to the fact that scattering cross section is effective only around the oscillation resonance frequency of a plasmonic particle. As mentioned above, this cross section is much larger than dimensions of the particle around resonance frequency and reduces abruptly as we go far from the resonance condition.

The size of the particles is not the only variable that defines the overall scattering property of the object. The use of core-shell configuration and other geometries, such as nanorod instead of a bare spherical particle, are other methods employed for tailoring the scattering efficiency of the system.<sup>[82]</sup> The ratio between scattering and absorption cross sections can be utilized as a measure to evaluate these different designs. Figure 6c shows this ratio for different configurations of scattering nano objects. As this panel implies the scattering capacity of the system takes its dominancy as we go to larger dimensions regardless of the object shape and its configuration. However, in the nanorod case, this ratio can be obtained in much smaller dimensions compared to that of nanosphere and it does not change considerably by changing the aspect ratio of the design. These results also prove that this ratio is the largest for the core-shell configuration, in which as the radius of shell layer increases the scattering becomes the main mechanism involved in the metal NP operation.

### 2.2.1.2. Optical Near Field Coupling

Another mechanism,<sup>[82]</sup> responsible for radiative energy transfer, is through optical coupling originated from near field evanescent modes. Unlike propagating far field modes, evanescent waves do not transport energy and, therefore, they can create large electric field amplitudes without violation of energy con-

servation. On the other hand, the confined nature of decaying localized plasmon modes confirms their near field evanescent behavior. This highly concentrated light in sub-wavelength geometries is called a hot spot. Many applications of plasmonic nanostructures indeed take advantage of the existence of these hot spots. The electric field distribution in the vicinity of a plasmonic design is a direct function of its shape. The shape does not only change the near field amplitude but also it modulates the spectral position of this peak. Figure 7a compares

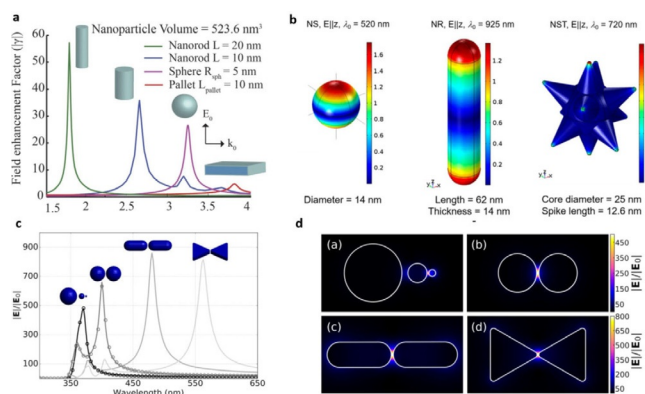


**Figure 7.** a) The field enhancement factor for different shapes of nano-plasmonic designs as a function of light wavelength (Reproduced with permission from Ref. [83]). Copyright 2015, Springer Nature). b) The electric field amplitudes and distribution on different plasmonic shapes (Reproduced with permission from Ref. [85]). Copyright 2016, American Chemical Society). c) The electric field amplitude and d) its distribution for different almost-touching plasmonic configurations (Reproduced with permission from Ref. [88]). Copyright 2016, American Chemical Society).

the near field enhancement between different structures including nanopallet, nanosphere, nanorod (NR), and nanowire (NW).<sup>[83]</sup> As this Figure implies, the field enhancement is the lowest for the case of pallet and sphere designs. Moreover, the spectral position of this peak is located at the UV region which has only 3% of the solar spectrum energy. The story, however, is different for the other elongated designs such as NRs and NWs. As the ratio between longitudinal and lateral dimensions gets larger both amplitude and resonance positions get improved where an efficient visible and NIR light harvesting can be possible. Hot spots can also occur at the sharp corners and edges of a design.<sup>[84,85]</sup> As shown in Figure 7b, the use of nanostars has been shown to be an excellent choice for light confinement in a small spatial position where an electric enhancement with an order of magnitude larger amount can be attained compared to that of a NW design.<sup>[85]</sup> This enhancement can be also probed within narrow gaps between metal NPs cluster. The enormous intensity enhancement factors associated with localized surface plasmons, up to several orders of magnitude, directly translate into an increase of electronic transition probabilities for atoms or molecules exposed to such fields. In other words, an extraordinary absorption cross section is provided in the vicinity of these nano resonant units. If a photoactive component, such as a photoanode in a water splitting process, is brought to the vicinity of this particle, a rel-

atively high concentration of electrons and holes would result. These photo-induced carriers are involved in photocurrent enhancement and overall performance of the PEC-WS system would be substantiated. The small spatial gap between aggregated nanostructures is one of the architectures that support the formation of hot spots. However, in this design, there is no control on the position of these highly focused points. Therefore, geometries with anisotropic sharp corners such as nanotriangles, NRs, and nanostars are desired structures for optimum light confinement.<sup>[84–86]</sup> These designs can offer spatial control for the formation of hot spots. However, the confinement is much more efficient in the case of nearly touching nano resonators where light is bounded in the small gaps. The coupling between these units is also a function of single element geometry. Figure 7c,d compares the electric field distribution intensity between two close nanostructure elements for different resonator shapes. This coupling has been compared with a self-similar chain design that is realized as an efficient hot spot generator. The cascaded field enhancement in a self-similar antenna of nano spheres was first introduced by Stockman.<sup>[84,87]</sup> In this architecture, the radii of the particles in the array scale as  $R_{n+1} = kR_n$  and the inter particle distances as  $d_{(n+1),(n+2)} = kd_{(n),(n+1)}$ , in which  $k$  is the scaling factor and  $n$  is the particle number. This geometry provides a multiplicative cascade effect in which the largest element intensifies the incident field by a factor of  $f$ , the enhanced field excites the next smaller particle which in turn enhances the field by another factor of  $f$ , and in this way the structure can provide a highly spatially confined spot. As this Figure shows, the field is concentrated in the gap of two units. This means that the configuration possesses an extraordinary absorption cross section in the vicinity of its surface which can be utilized to create electron/hole pairs to boost the photocurrent amount in the PEC-WS cell. Better qualitative comparison on the light confinement ability of the design can be provided by considering the near field electric field enhancement of each of these designs. As Figure 7c illustrates, the strongest response belongs to the NR case, which is about two times larger compared to that of the self-similar design. Therefore, taking near field enhancement as one of the prominent factors in defining the effectiveness of a design, NRs with a proper proximity can be the most promising option for a hot electron driven PEC-WS system. However, the strength is not the only variable that matters. Another Figure of merit for a photo active material is the bandwidth of the operation that can be evaluated as full width at half maximum (FWHM). This factor is the best in the case of a bowtie structure, although it is not too different. The last property that defines the functionality of a nano resonant unit is its spectral position of the resonance unit. This property is directly related to the shape, size, and composition of the plasmonic design. Although this near touching resonators have the highest light confinement capacity, their fabrication generally needs to e-beam lithography which is a complex process and has large scale compatibility issues. Therefore, it is envisioned that the use of chemically synthesized nanostructures is the most promising approach in design of a highly efficient PEC-WS cell.

## 2.2.2. Nonradiative Energy Transfer

In this type of energy transfer, the plasmonic structure contributes to photocurrent enhancement by directly injecting its electron into the conduction band of the semiconductor. Different from radiative energy transfer process, this process can harvest the entire visible light spectrum regardless of the band gap of the substrate semiconductor. In other words, the unique property of below band gap absorption and electron generation in plasmonic structure depends on the efficiency of this process. This mechanism can be classified as two main transfer processes; (1) hot electron injection, and (2) plasmon resonant energy transfer. In the following section, these two processes will be discussed in detail.

### 2.2.2.1. Hot Electron Injection

One of the responsible mechanisms for photocurrent enhancement is hot carrier injection. Upon the excitation of plasmonic metal, the LSPR gets excited. The nonradiative decay of LSPR can generate hot carriers. The initial distribution of electrons and holes does not follow Fermi-Dirac distribution and they decay according to the Landau damping process (Figure 8a).<sup>[75]</sup>

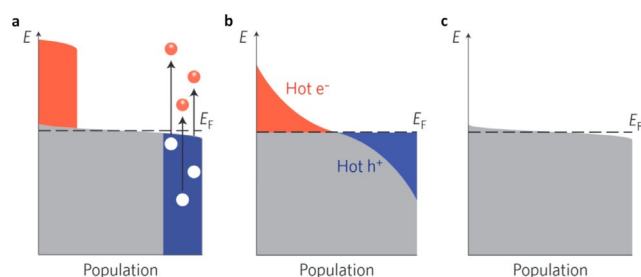


**Figure 8.** Ultrafast direct hot electron transfer mechanism in a plasmonic design. a) The initial distribution of electrons and holes that does not follow a Fermi-Dirac distribution. b) Electron-electron scatterings redistribute the energetic location of electrons and the Fermi-Dirac distribution is again formed. c) Finally, the system is cooled down and electrons come back to their initial state. Reproduced with permission from Ref. [75]. Copyright 2015, Springer Nature.

During this process, the large density of hot carriers is within energy levels close to  $E_F$  (within a few tenth of eV) and only a portion of these carriers has enough energy to pass the Schottky barrier and contribute to photocurrent.<sup>[89]</sup> However, this initial hot electron distribution is not in equilibrium and e-e scatterings redistribute the energetic location of electrons and the Fermi-Dirac distribution is again formed but this time the equivalent Fermi energy level ( $E_F$ ) is at more energetic levels, see Figure 8b.<sup>[90,91]</sup> Although the lifetime of hot carriers for each energy level is in the order of tens of fs, relaxing from the non-equilibrium distribution to a Fermi-Dirac one takes hundreds of fs. It has been found that electrons within 1 eV of the Fermi level have lifetimes around 100 fs, but this time reduces to 10 fs for electrons with energetic locations of above 3 eV.<sup>[92]</sup> Similar to electrons, holes close to sp-band have less

scattering compared to ones in the proximity of d-band, which prolongs their lifetime.<sup>[79]</sup> This state is a hot thermally equilibrium state and it needs to dissipate its energy to come back to the initial state, as shown in Figure 8c. This occurs during the relaxation of hot carriers by transferring the additional energy to the vibrational motions of the nuclei via electron-phonon interactions. During this process, electrons are cooled down to the nuclei temperature. The time scale of this step is generally a few ps and it is tailored with plasmonic metal geometry and size together with the substrate material, wherein plasmonic design is located on it. As mentioned in the near field coupling section, the plasmonic response of different nanostructures can be tuned with their shape. Although NWs were found to be an excellent light harvesting design, their hot electron injection efficiency is not as promising as their near field enhancement. As depicted in Figure 9b, the injection efficiency has the highest value for the case of nanospheres that makes them an excellent choice for hot electron driven systems.<sup>[83]</sup> To be able to use these hot carriers, they need to be injected to the semiconductor before they return to their initial states. Considering the fact that lifetime of these carriers is ultrashort, the overall efficiency of this injection is quite short. In a typical architecture, a plasmonic metal is brought into contact with an

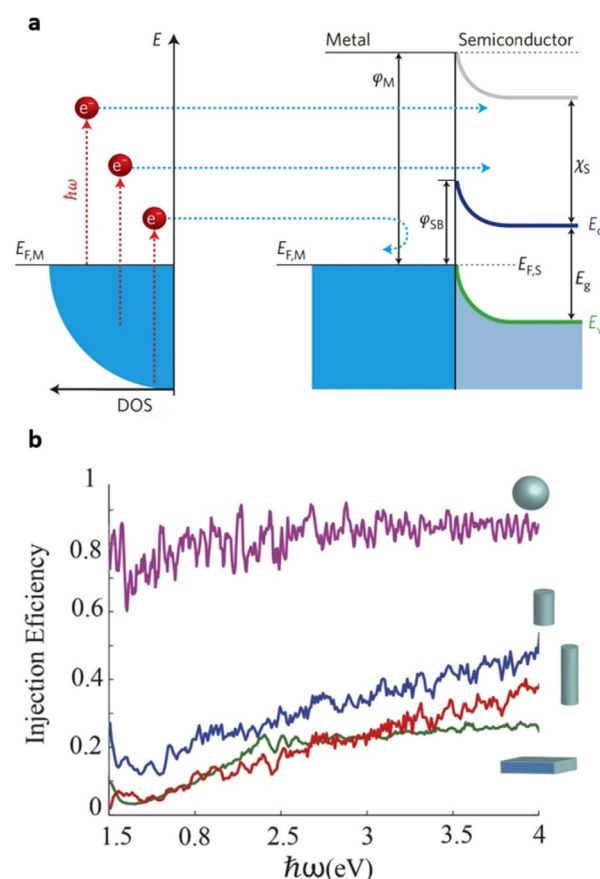


**Figure 9.** a) The hot electron generation and injection process at a metal-semiconductor interface (reproduced with permission from Ref. [74], copyright 2014, Springer Nature) and b) comparison of the injection efficiency of different plasmonic shapes (reproduced with permission from Ref. [83], copyright 2015, Springer Nature).

acceptor, which is typically an n-type semiconductor. As Figure 9b shows the interface of a metal–semiconductor hybrid forms a Schottky junction, if the  $E_F$  of the metal is located within the semiconductor band gap. This junction sets a barrier for electron transfer from metal to semiconductor. If an electron has enough energy to pass this barrier (or tunnel through it), it can be collected with semiconductor material. The formation of this barrier significantly mitigates electrons back reaction that makes this process efficient. This barrier depends on the  $E_F$  position of plasmonic metal and for a typical Au–TiO<sub>2</sub> junction it is about 1 eV. However, the density of energetic electrons that can pass this barrier is quite low. Moreover, as mentioned earlier, the density of electrons can be significantly improved by reducing NPs size. The introduction of hot spots can be also a promising approach to increase the efficiency of this process. However, these energetic hot electrons have much smaller lifetimes compared to that of close to the  $E_F$  level. Additionally, the time scale for injection of a hot electron to the neighborhood semiconductor is a function of the metal–semiconductor interface. It has been experimentally demonstrated that this time scale is in the order of 50 fs for Au–TiO<sub>2</sub><sup>[93]</sup> and 20 fs for Au–CdS.<sup>[94]</sup> Therefore, a proper design is required to improve the efficiency of this process. That is why the efficiencies have generally been limited to an amount below 10% for a metal–semiconductor junction. One of the ways that can enhance the injection probability of these carriers is to increase the contact area between plasmonic NPs and the semiconductor. Moreover, taking the short diffusion length of carriers inside the metal, the dimensions of these particles should remain small. However, this architecture increases the probability of recombination of electrons, in which hot carriers can back react with hot holes inside the metal. This probability can be intensified considering the existence of trap level on the semiconductor surface. During the hot electron injection process, these surface traps can trap these carriers and mediate recombination path. It has been experimentally and theoretically proven that interface engineering with an angstrom thick embedded layer can significantly passivate surface traps without hindering electron tunneling probability.<sup>[95–99]</sup> It has been shown that first cycles of an atomic layer deposited (ALD) metal oxide on TiO<sub>2</sub> surface can passivate surface oxygen vacancy trap states. Substantial layers, however, impeded injection probability of photogenerated carriers exponentially. Therefore, it is envisioned that use of a subnanometer interfacial layer can greatly substantiate hot electrons extraction.

### 2.2.2.2. Plasmon Resonant Energy Transfer

Another mechanism responsible for nonradiative energy transfer of hot electrons is plasmon-induced resonance energy transfer (PRET). In this process, the decay of surface plasmons induces electron/hole pairs directly in the semiconductor via dipole–dipole interactions with a transient exciton (Figure 10a). The overlap between plasmonic metal and semiconductor conduction band defines the efficiency of this transfer. The rate of this transfer can be analytically found as [Eq. (4)].<sup>[91,92]</sup>

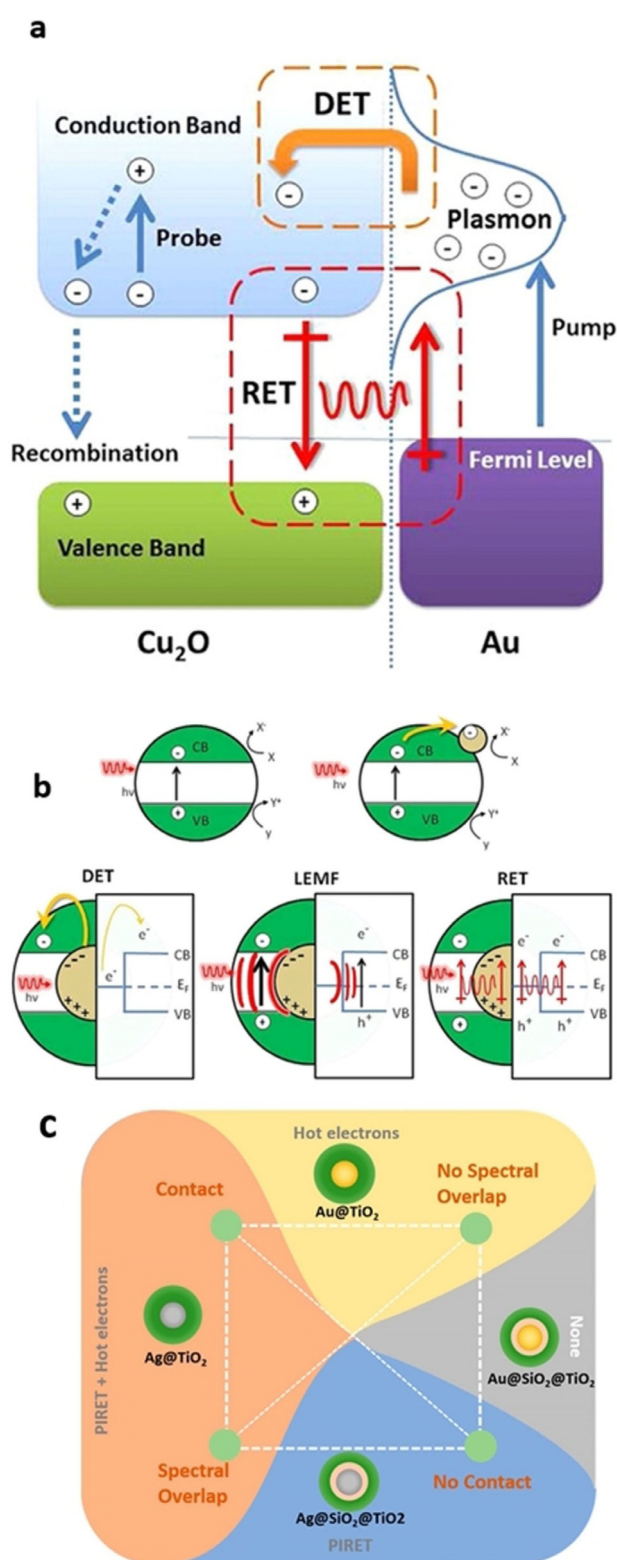


**Figure 10.** a) The set of processes involved in a PRET energy transfer for an Au–Cu<sub>2</sub>O interface. Reproduced with permission from Ref. [100]. Copyright 2012, American Chemical Society. b) The differences of energy transfer in three different processes of direct hot electron transfer, localized electric field coupling, and plasmon resonance energy transfer. Reproduced with permission from Ref. [100]. Copyright 2012, American Chemical Society. c) The responsible plasmonic energy transfer mechanisms for four different metal–semiconductor composition configurations. Reproduced with permission from Ref. [101]. Copyright 2015, American Chemical Society.

$$k_{\text{transfer}} = \frac{1}{\tau_{\text{metal plasmon}}} \left( \frac{R_0}{r} \right)^6 \quad (4)$$

where  $\tau_{\text{metal plasmon}}$  is the lifetime of an isolated metal carrier,  $r$  is the distance between plasmonic metal and semiconductor, and  $R_0$  is a constant that depends on the material properties of the system and their spectral overlap. As the formula clearly illustrates, unlike the hot electron injection process, the transfer does not need a direct contact between metal and semiconductor. It should be mentioned that the involved mechanism in this phenomenon is different from that in radiative optical near field coupled electron/hole pair generation. This can be clarified through a comparison among three different processes, as shown in Figure 10b.<sup>[100]</sup> In the hot electron injection process, the generated electrons are directly transferred into the adjacent semiconductor. In the near field coupling, originated from radiative emission of plasmonic hot electrons, the near field evanescent modes activate the neighborhood semiconductor. In this reaction, the photon requires an energy above the semiconductor band gap to create electron/hole pairs. Unlike this mechanism that create carriers only for energies above the band gap of semiconductor, PRET directly excites free carrier nonradiatively through the relaxation of localized surface plasmon dipole for above and below band gap photons. The efficiency of this process has a close relationship with the composition of the metal-semiconductor hybrid design. Wu and co-workers conducted transient absorption spectroscopy on four different core-shell metal nanospheres including, Au-TiO<sub>2</sub>, Au-SiO<sub>2</sub>-TiO<sub>2</sub>, Ag-TiO<sub>2</sub>, and Ag-SiO<sub>2</sub>-TiO<sub>2</sub>, to study different energy transfer mechanisms in each of these hybrid designs.<sup>[101]</sup> Figure 10c demonstrates that hot electron injection is the dominant process in Au-TiO<sub>2</sub> NPs following light absorption due to direct contact between metal and semiconductor, whereas the PRET process was not supported in this design that is due to lack of spectral overlap between gold absorption and TiO<sub>2</sub> absorption tail. Embedding a thin SiO<sub>2</sub> shell in between, both mechanisms get deactivated due to missing direct contact. However, proper overlap between Ag and TiO<sub>2</sub> makes this design as an excellent core-shell structure for plasmonic based water splitting system. Finally, the Ag-SiO<sub>2</sub>-TiO<sub>2</sub> ternary design just stimulates the PRET process.

### 3. Recent Strategies for Hot-Electron-Driven PEC-WS

In this section, the strategies employed to improve plasmonic-based water splitting have been categorized and discussed in three sub-sections: 1) nanoplasmonic units, 2) nanostructure support scaffolds, and 3) interface engineering of the design.

#### 3.1. Nanoplasmonic Units

##### 3.1.1. Shape

As mentioned above, one of the most important parameters defining the effectiveness of the system is the shape and ge-

ometry of the plasmonic unit. The most commonly used plasmonic unit is considered to be spherical (or semi spherical) NPs and several studies have utilized this design.<sup>[102–130]</sup> However, these NPs typically provide the SPR absorption in a specific frequency range around  $\approx 550$  nm and they cannot be utilized fully in the solar spectrum (Figure 11).<sup>[131]</sup> This is an important

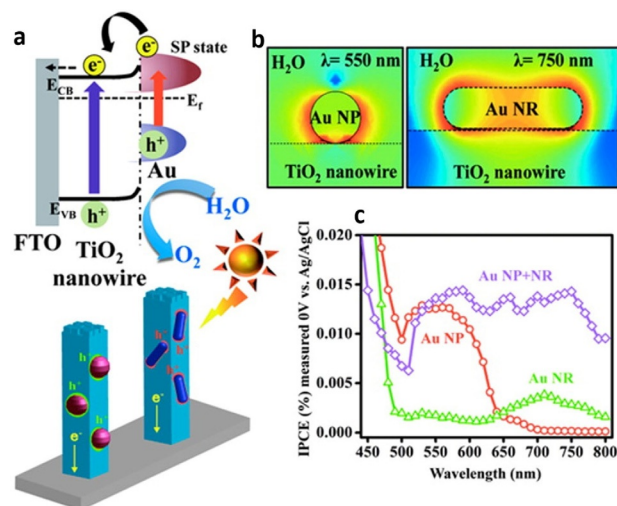


**Figure 11.** a) The electron injection process in an Au-TiO<sub>2</sub> composite where the Au nano units are NPs and NRs. b) A comparison on the electric field distribution and formation of hot spots in NPs and NRs structures and c) their corresponding IPCE profiles. Reproduced with permission from Ref. [131]. Copyright 2013, American Chemical Society.

factor where the use of broader nanoplasmonic units can create higher density of hot electrons to be injected into semiconductor transport layer. To be able to extend light absorption spectra toward the NIR region, the unit should be elongated in one dimension. This has been proven in other plasmonic based devices.<sup>[132]</sup> In this case, the structure can support two fundamental modes corresponding to transverse and longitudinal dimensions. Moreover, it has been demonstrated that electric field distribution in NR structure provides stronger hot spots. This intense electric field can improve PEC device performance by providing an efficient electron-hole pair separation, stronger PRET process and hot electron injection. It was found that the combination of NRs and NPs of Au can provide light absorption in both visible and NIR region.<sup>[131]</sup> The incident photon conversion efficiency (IPCE) results revealed that NPs enhance the photocurrent values in a 450–650 nm range but the NR case shows its response in the NIR regime (between 650 nm and 900 nm). Moreover, the near electric field amplitude shows different intensities for NP and NR cases. While the NP decorated TiO<sub>2</sub> proves an enhancement in the order of 5 times, this value is recorded to be 15 times in the case of NR plasmonic Au unit. The similar results have been obtained with other studies where the use of Au NRs can provide broader spectral response and higher near field enhancement facilitating the hot electrons injection into adjacent semiconductor.<sup>[133]</sup> As mentioned in the previous sections, the stronger hot spots can be seen in the morphologies with sharp corners.<sup>[85]</sup> Calcu-

lated absorption, scattering and extinction spectra show that, although NP plasmonic structure can support a single relatively narrow mode, the use of nanocube provides multiple modes corresponding to dipolar, quadrupolar, and other higher order ones associated with the corners of the design.<sup>[84]</sup> The superposition of these modes has caused the overall response to be broad covering the whole visible spectrum. The similar spectral response is recorded for nanopyramids but the weaker overlap between these modes makes the overall response to be a multiple narrow band one. Moreover, the plasmonic synthesized structures are not the only choices to get plasmon enhanced water splitting. Some reports have revealed the possibility of all plasmonic systems for PEC-WS application where the bulk material is a bulky plasmonic nanostructure.<sup>[134, 135]</sup> In these designs, the Au NRs have been utilized to provide generation of hot electron/hole pairs in a wide frequency range. These NRs are partially coated with electron extraction layer such as TiO<sub>2</sub> and an oxygen evolution catalyst. Upon excitation of LSPR in the Au NR and its nonradiative decay, the hot carriers are generated inside the Au bulk. The electrons are transferred into TiO<sub>2</sub> to perform HER. The remaining hot holes are accumulated in the oxygen evolution catalyst to oxidize water and create O<sub>2</sub> gas.

### 3.1.2. Size

Another important factor affecting the overall water splitting process is the size of plasmonic NP. As we explained earlier in the introduction section, the hot carrier generation and its transport distance is directly influenced with the particle size and dimension. The size of plasmonic metal governs the efficiency of plasmon induced hot electron transfer. As Figure 12a shows, to elucidate the mechanism responsible for water reduction under the use of different sized NPs (4.4 nm and 67 nm), two different light sources ( $\lambda > 400$  nm and  $\lambda > 435$  nm) were utilized.<sup>[123]</sup> Figure 12b explains that upon excitation with  $\lambda > 400$  nm source, the small NPs show significantly higher hydrogen production capacity compared to that of big ones while for  $\lambda > 435$  nm, the large Au NPs represents high activity and no hydrogen molecule is detected for the small ones. The hydrogen evolution activity of the system under only visible light irradiation depends on the SPR strength in the metal-semiconductor interface (because the TiO<sub>2</sub> support cannot be activated). It is known that this effect is much higher for the larger plasmonic particles and small particles have much smaller strength. Upon the excitation of the Au SPR with  $\lambda > 435$  nm, intense SPR-enhanced EM fields are generated on the Au NP surface significantly increases the yield of interfacial "hot electrons" with a higher potential energy than  $\phi$  at the interface, which in turn induces fast and efficient transfer of "hot electrons" to the conduction band of semiconductor, see Figure 12a. Since, under this condition, TiO<sub>2</sub> is not excited, the electrons injected to semiconductor would have longer lifetime to transport. However, for  $\lambda > 400$  nm excitation case, this recombination impedes the electron lifetime and consequently less hydrogen will be generated. The activity of the small NPs in this case has been attributed to electron

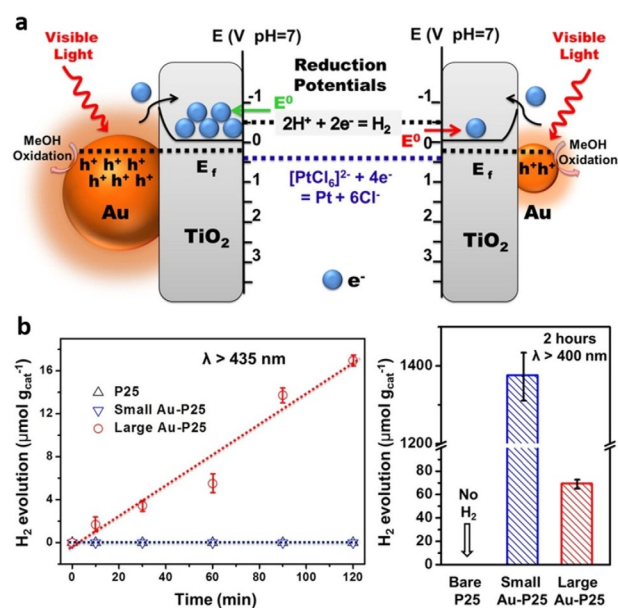


**Figure 12.** a) The mechanisms responsible for hydrogen generation for small and large Au NPs under visible light irradiation. b) The amounts of evolved hydrogen gas for small and large NPs under two different sources of incident light irradiation. Reproduced with permission from Ref. [123]. Copyright 2014, American Chemical Society.

transfer from semiconductor conduction band to metal Fermi level in which this local separation reduces the recombination rate of the semiconductor. Moreover, the conducted investigations have shown that the chemical reduction potentials are also a function of the particles size. The injection of electrons from metal to semiconductor builds up a high concentration of electrons and this brings the potential level to higher values than the H<sub>2</sub> evolution potential. Therefore, considering the stronger SPR mediated hot electron transfer in larger particles, they have more suitable condition to evolve hydrogen. Even at the SPR regime, where the particle size is couple of tens of nanometers, the photocatalytic performance of the plasmonic metal can be tuned. In fact, the localized SPR frequency of a metal can be tailored by adjusting its size. From spectral line shape of a metal, one can analyze the spectral peak position ( $E_{\text{LSPR}}$ ) and its full wave half-maximum ( $\Delta\lambda_{\text{FWHM}}$ ). The change on these parameters can influence the local field enhancement which is an important phenomenon defining overall performance of a PEC-WS system. This effect has been scrutinized in a study, where precisely controlled Au nanodot with dimensions of 50 nm, 63 nm, and 83 nm were utilized for plasmon enhanced PEC cell.<sup>[121]</sup> To be able to provide a qualitative comparison on the field enhancement capacity of these particles, the quality factor (defined as  $Q = E_{\text{LSPR}}/\Gamma$  where  $\Gamma$  is found from Plank's equation ( $E = pc/\Delta\lambda_{\text{FWHM}}$ )) of these particles have been compared as shown in Figure 13. As this figure suggests that the Q factor of the particles gets larger amplitudes as we go to smaller ones. This large value proves higher local field enhancement, in which larger photo induced carriers will be created and consequently the photocurrent values rise up. As implied in this paper, under visible irradiation (with light intensity

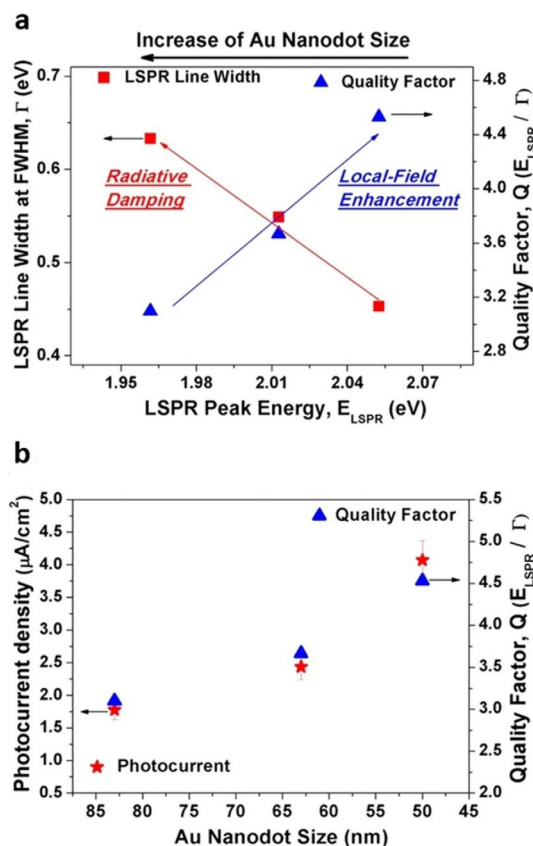


**Figure 13.** a) The dependence of the quality factor, LSPR energy and its FWHM on different NP sizes. b) The impact of plasmonic Au NP size on the quality factor and the generated photocurrent densities of the corresponded PEC-WS device. Reproduced with permission from Ref. [121]. Copyright 2014, American Chemical Society.

of  $122.5 \text{ mW cm}^{-2}$ ) the photocurrent values have been improved by 10 times for 83 nm sized Au dots while it is about 25 times for the 50 nm case. The optimum particle size is also a function of the main mechanism responsible for photocurrent generation. This has been proven in a recent study on the use Au-BiVO<sub>4</sub> combination for PEC water splitting.<sup>[116]</sup> Sweeping the NP size from 10 nm to 80 nm, it was found that the highest response is obtained for the 30 nm size case. It was demonstrated that the main mechanism responsible for water splitting enhancement is the generation of electron/hole carriers in BiVO<sub>4</sub>, due to high near field light coupling. As the particle size gets larger, a red shift is recorded for the plasmonic spectra of the particle. Therefore, the overlap between the absorption edge of BiVO<sub>4</sub> and Au plasmonic particle gets narrower and fewer carriers are generated. Moreover, larger particles hinder the exposed area of semiconductor to electrolyte, which can diminish the water oxidation efficiency on the BiVO<sub>4</sub> surface. Therefore, the function of particle size also depends on the support substrate, in which a narrow band gap semiconductor can make the PRET process and near field optical coupling an efficient mechanism for activity enhancement of the design.

### 3.1.3. Composition

Rather than a bare single plasmonic metal, the use of metal-metal, metal-semiconductor, and metal-insulator composite can provide a performance enhancement by tailoring the absorption/scattering strength and bandwidth. Bimetallic design, where two metals are brought in contact in a core-shell configuration, can offer several optical and electrical properties that cannot be attained by a monometallic structure,<sup>[136,137]</sup> (1) broader spectral absorption bandwidth of the design due to multiple plasmon resonances of different metals, (2) intense light spatial confinement to boost electron-hole pair generation, (3) stronger light scattering, and (4) less ohmic losses by tailoring the radiative damping ratio of the lossy metals. It has been demonstrated that Au-Ag core-shell nanosheets, embedded within the mesoporous TiO<sub>2</sub> photoanodes, can propose much higher photocurrent density relative to the bare Au-TiO<sub>2</sub> photoanode design. The enhancement in the cell performance has been attributed to the existence of dual resonance modes from these two metals, strong near field coupling of the plasmons, and better charge separation and transfer through the interface and inside of the TiO<sub>2</sub> semiconductor.<sup>[64]</sup> Based on Mie theory, the coating of a metal with a semiconductor structure can also enhance its SPR interaction with light.<sup>[119,121]</sup> Moreover, employing a semiconductor with proper band alignment can provide an efficient charge separation at the metal-semiconductor interface. In all the above mentioned heterostructures, the plasmonic NP is fully coated with the semiconductor shell. In this configuration, hot electrons are injected to titania and are involved in photoreduction reaction but holes cannot take place in oxidation reaction, due to sluggish kinetics of this reaction. Wu et al.<sup>[133]</sup> have developed a novel wet chemistry synthesis method, as shown in Figure 14, to make AuNR-TiO<sub>2</sub> nanodumbbells in which the plasmonic Au is partially coated with TiO<sub>2</sub>. The injection of electrons from Au particle to the TiO<sub>2</sub> shell conducts the reduction process and at the meantime, the charge balance is restored through the oxidation reaction occurred at the bare surface of Au NR. This has been demonstrated to be much more effective for PEC-WS application compared to that of an entirely coated Au NR design. The same methodology has been used in a CdS based system. In the proposed study, a hybrid heterostructure of Au-CdS core-shell has been synthesized for this aim.<sup>[138]</sup> The shell is made of tightly packed 3–5 nm quantum dots coated on a 14 nm Au NP. Owing to its optimized band gap and band positions, CdS is an excellent semiconductor for overall water splitting process. However, the use of this material is impeded due to its lack of photo stability. In this design, Au core acts as a hole scavenger for the photo generated carriers inside the CdS shell and hinders its corrosion. This mechanism is not only useful for providing photo stability but also it introduces a proper route to separate carriers and reduces their recombination probability. The results of this paper reveal that hot electron injection due to excitation with a visible light  $\lambda \geq 500 \text{ nm}$ , cannot be an effective way to improve the hydrogen evolution reaction rate. In another study, this core-shell configuration has been employed on a SrTiO<sub>3</sub> support.<sup>[139]</sup> As

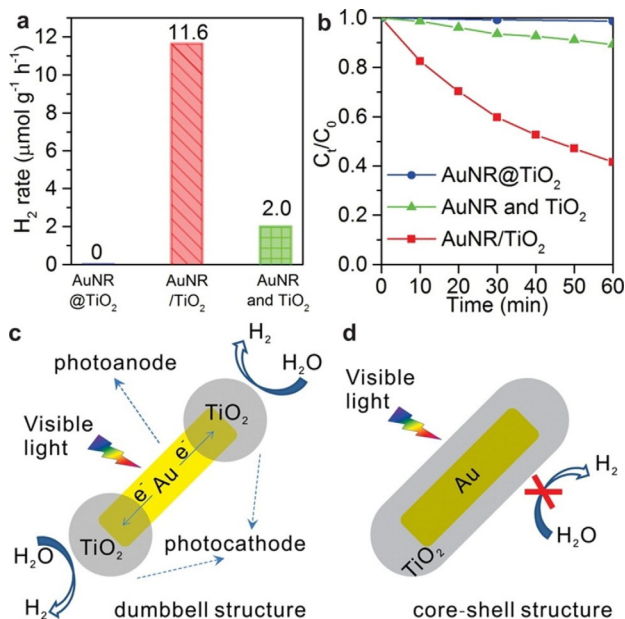


**Figure 14.** Comparison of a) the HER activities and b) normalized concentration of the dye vs. irradiation time under visible illumination and in the presence of methanol and water. The corresponded operation mechanisms for c) partially coated dumbbell shaped and d) core-shell Au-TiO<sub>2</sub> composites. Reproduced with permission from Ref. [133]. Copyright 2016, American Chemical Society.

depicted in Figure 15, in this design the electrons follow a pathway from CdS to Au and then from Au to SrTiO<sub>3</sub> where the conduction band of this semiconductor is favorable for H<sub>2</sub> evolution. The clear fact in the aforementioned compositions is that the formation of a shell layer around the metallic core is mainly employed to boost the injection efficiency of hot electrons. The injection of hot holes can also be modified to a more efficient way using a co-catalyst such as IrO<sub>x</sub>.<sup>[129]</sup>

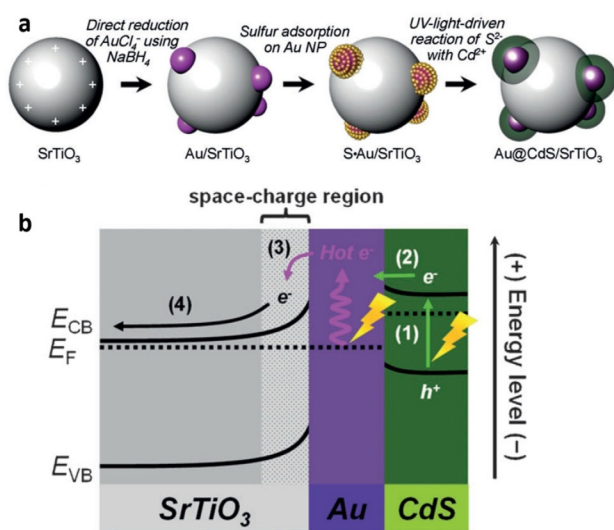


**Figure 15.** a) The preparation route and b) electron transfer dynamics in a CdS-coated AuNPs-SrTiO<sub>3</sub> multi-junction design. Reproduced with permission from Ref. [139]. Copyright 2014, Wiley-VCH.

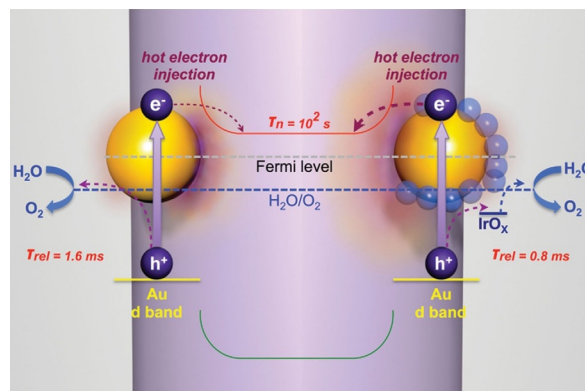


**Figure 16.** The electron- and hole-transfer dynamics of an AuNP plasmonic unit in the presence of an IrO<sub>x</sub> co-catalyst. Reproduced with permission from Ref. [129]. Copyright 2016, Wiley-VCH.

Figure 16 proves that this OER co-catalyst can mediate the interfacial charge transfer between electrolyte and surface of plasmonic NPs (gold; due to its valence band position located in between). Along with improving the sluggish reaction rate of the oxidation process, this separation boosts hot electron injection process as well.

### 3.2. Nanostructured Support Scaffolds

One of the most prominent factors influencing the overall efficiency of a water-splitting cell is the configuration of the support scaffold where plasmonic metal is coated. In a typical design, metal NPs are attached on a bulk semiconductor<sup>[116, 119, 121, 123, 127, 140–143]</sup> or an insulator,<sup>[85, 109, 110]</sup> in which in some of the configurations the semiconductor is a porous structure.<sup>[116, 119, 123, 141]</sup> In this design configuration, the generated hot electrons are injected into semiconductor layer and transported toward counter electrode where the HER takes place. On the other hand, the OER process is realized on the surface of plasmonic metal. Therefore, the overall PEC-WS strongly depends on the surface area of the semiconductor and, therefore, a bulky design (with a small surface area) is not an efficient choice for the photoanode design. Moreover, in a bulk design, fewer particles are loaded on the semiconductor and consequently a smaller density of electrons is obtained. Besides these drawbacks, this design does not have the capability to trap the light inside the design and during the light passage through the design, only a part of incident light is absorbed with the metal NPs. All of these deficiencies are suppressed by employing a properly designed nanostructure. A nanostructure architecture can be one-dimensional (1D) such as NWs,<sup>[103, 131, 144]</sup> NRs,<sup>[102, 111, 125, 129, 134, 145, 146]</sup> and nanotubes (NTs),<sup>[117, 118]</sup> or a three-dimensional (3D) scaffold like branched structures, nanocones, and so on. The use of nanostructure support semiconductor scaffold has been the subject of many studies in the field of plasmonic PEC WS. Ideal solar-to-fuel convertor must efficiently harvest sunlight to generate significant quantities of long-lived charge carriers necessary for chemical reactions. However, as already mentioned, the main limiting factor for this process is the short lifetimes of photo-

generated electron-hole pairs. The use of these nano designs increases both density of photogenerated carriers and reaction surface area and this in turn leads to conversion efficiency enhancement. In this section, different nanostructures for PEC-WS application are reviewed.

The use of TiO<sub>2</sub> NW and NR array as the support and Au NP as the plasmonic sensitizer is one the most commonly employed designs for PEC WS. In this Scheme, the semiconductor nanostructure is served solely as a conduit for hot electron transport. This NWs topology has been proved to improve PEC performance by decoupling the directions for light absorption and charge transport within the device, while providing an uninterrupted conductive corridor for charge carriers to reach the back contact. Under visible light irradiation, Au-TiO<sub>2</sub> heterostructure can create a large density of photogenerated carriers in which the plasmonic NPs act as light harvesting assemblies and transfer the hot electrons into semiconductor design through the PRET and hot electron injection processes. These hot carriers have lifetimes of one to two orders of magnitude longer than those of TiO<sub>2</sub> generated via UV excitation.<sup>[103]</sup> This is mainly due to formation of Schottky barrier in the metal/semiconductor interface which impedes electrons back transfer and consequently reduces their recombination rate.<sup>[103]</sup> Moreover, this recombination reduction has also been assigned to the surface passivation of semiconductor by using gold NPs.<sup>[103,131]</sup> Similar results have also been reported for ZnO-Au heterostructure.<sup>[105,146]</sup> The match-like heterostructure with Au NPs coated on the tip of ZnO NRs exhibits high plasmon enhance light absorption together with better charge separation and transport. The current density for this design is found to be 9.11 mA cm<sup>-2</sup> at an applied voltage of 1 V (vs. Ag/AgCl) that was much higher compared to that of a pristine NR array (0.33 mA cm<sup>-2</sup>).<sup>[146]</sup> Interestingly, it was shown that the stability of the design is also improved for the metal coated structure which is a major drawback for ZnO based cells. The accumulation of the holes at the ZnO NR results in its photocorrosion. However, Au NPs can efficiently separate electrons and holes and consequently reduce surface photocorrosion. The use of nanopencil array of ZnO is another strategy to improve the overall efficiency and stability of the cell. In this structure, the NR is narrowed to a needle-like tip where generated carriers need to pass shorter distance to reach to the semiconductor-electrolyte interface. Moreover, the energy transfer through the PRET process intensifies the electric field intensity in a small part of semiconductor structure. The Au-ZnO nanopencil heterojunction array provides a photocurrent of  $\approx 1.5$  mA cm<sup>-2</sup> at an applied voltage of 1 V (vs. Ag/AgCl).<sup>[105]</sup> Ag microflowers decorated on top of Si microwires were also demonstrated to be an efficient photocathode for water splitting.<sup>[144]</sup> Therefore, the essential goal of using these nanostructures is to increase the surface area of the design. This can be attained by reducing the NWs radius or increasing their density. However, the carrier diffusion length becomes significantly shorter when the radius gets smaller. A better strategy is to use 3D branched structures where smaller and thinner branches are attached to the vertically aligned NWs.<sup>[106,108]</sup> By using this design configuration, not only the surface area and the gold NPs loading in-

crease but also the light harvesting capability of the design is enhanced. Zhang et al. employed Au-ZnO branched nanostructure and obtained a photoconversion solar-to-hydrogen efficiency as high as 0.52% under simulated sunlight illumination.<sup>[108]</sup> It has been shown that, although the absorbance values for bare ZnO NWs and branched ZnO NWs are quite close to each other, Au loaded samples have much greater visible light absorption capacity compared to that of pristine NWs coated with Au plasmonic particles. Moreover, the obtained architecture, both the branches and the backbone, are single crystalline structures, which make them an excellent transport corridor for injected electrons. As illustrated in Figure 17, simi-

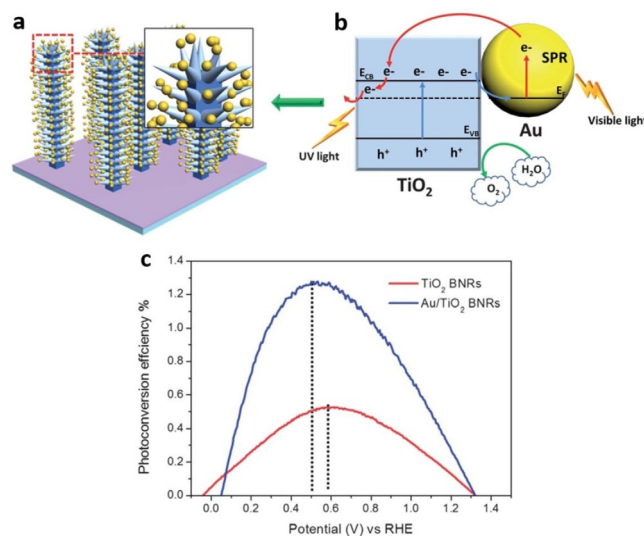


**Figure 17.** The a) design architecture, b) operation principle and c) STH conversion efficiency of a branched TiO<sub>2</sub> nanostructure coated with AuNPs. Reproduced with permission from Ref. [106]. Copyright 2013, Royal Society of Chemistry.

lar findings have been reported for the case of dendritic Au-TiO<sub>2</sub> NR arrays. Large surface area, efficient charge separation, and high carrier density (6 times compared to that of bare TiO<sub>2</sub> NR ones) have revealed one of the highest reported photoelectrochemical activities with a solar to hydrogen (STH) efficiency as high as 1.27%, as shown in Figure 17b. This heterostructure provides a photocurrent of 2.32 mA cm<sup>-2</sup> at a potential of 0 V vs. Ag/AgCl, under AM 1.5 G illumination (100 mW cm<sup>-2</sup>).<sup>[106]</sup> Employing nanorod-nanoplatelet hybrid design of ZnO is another design architecture that has been proved for enhancing the PEC-WS capability of the cell where a photocurrent density of 1.17 mA cm<sup>-2</sup> is achieved at a bias value of 0.6 V.<sup>[120]</sup> The maximum STH efficiency for this design is reached to 0.69%. In all of these designs, the plasmonic unit is loaded on the surface of nanostructure design and considering the wide band gap of ZnO and TiO<sub>2</sub>, hot electron injection is the main mechanism responsible for PEC performance enhancement of the cell in the visible portion of the spectrum. In a wise design, Li et al. demonstrated that the incorporation of visible light responsive hematite (Fe<sub>2</sub>O<sub>3</sub>) NRs into a plasmonic gold nanohole array pattern can significantly substantiate the PEC performance of

the design.<sup>[145]</sup> It was shown that the incorporation of this plasmonic design can lead to an approximately ten-fold increase in the photocurrent value compared to that of bare hematite NRs. Considering the visible light response of hematite semiconductor, the proposed periodic array of plasmonic nanohole design is responsible for PEC performance enhancement at the energy values below the band edge of the hematite NR. Above the band edge, however, the surface plasmon polaritons launch a guided mode through the length of NRs and this mode gets absorbed inside of it creating a high density of electron-hole pairs. Moreover, due to the strong light amplification inside the plasmonic nanohole, an efficient charge carrier separation leads to less recombination. This design provides an efficient strategy to utilize both photonic and plasmonic energy transfer for covering a wide spectral regime from UV to NIR.<sup>[145]</sup> TiO<sub>2</sub> NTs have been also shown to be a promising scaffold for the water splitting.<sup>[118]</sup> Although all of the above mentioned designs could efficiently transfer holes to the semiconductor-electrolyte interface, due to low conductivity (or low mobility) of TiO<sub>2</sub>, electrons collection efficiency is rather low. Therefore, a core-shell heterostructure, where the core material is a good electron conductor, could be a beneficiary for better charge separation and transport. In a recent study, authors have fabricated a core-shell configuration of aluminum doped ZnO (AZO)-TiO<sub>2</sub> as the semiconductor substrate for Au NPs.<sup>[114]</sup> Figure 18a reveals the preparation route of this design. The proposed multilayer design has been grown on periodic Al nanocone array as the scaffold. The use of nanocone pattern is not only advantageous for charge separation and transport, but it can also propose a good light trapping property, as it can be clearly revealed from Figure 18b. The IPCE findings of this study reveal that the enhancement in the PEC performance of the cell in the UV regime is due to optimal density of particles and their strong electric field confinement. However, the visible response of the system is originated from injection of hot electrons induced by localized surface plasmons. The PEC STH efficiency of this multi-junction design is found to be 0.73% at a low potential of 0.21 V vs. RHE. In another innovative design, as shown in Figure 19, Zhang et al. proved the

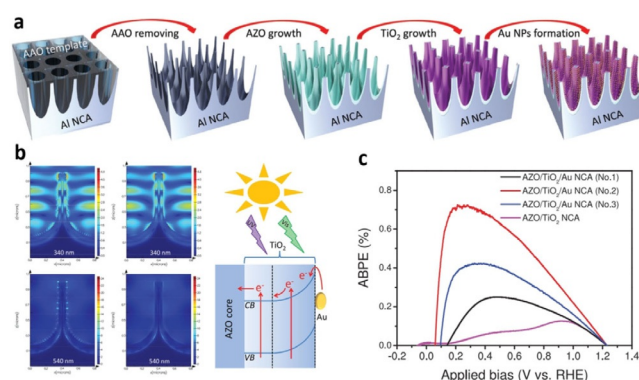


**Figure 18.** The a) preparation route, b) operation principle and electric field distribution, and c) conversion efficiency of periodically designed plasmonic AuNP-loaded nanocones. Reproduced with permission from Ref. [114]. Copyright 2015, Wiley-VCH.

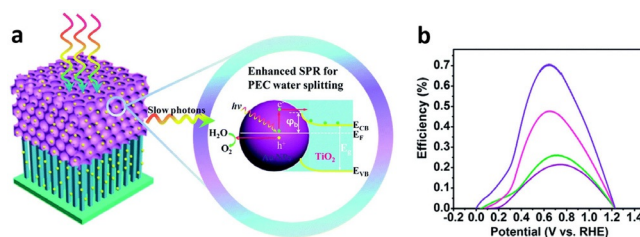


**Figure 19.** The a) mechanism responsible for the operation of a photonic crystal combined Au-TiO<sub>2</sub> NR plasmonic design and b) its STH conversion efficiency. Reproduced with permission from Ref. [102]. Copyright 2014, Royal Society of Chemistry.

use of coupling surface plasmon resonance of gold NPs with slow-photon-effect of TiO<sub>2</sub> photonic crystals for synergistically enhanced PEC water splitting system, in which a STH efficiency of 0.71% (at 0.64 V vs. RHE) was attained, (see Figure 19b).<sup>[102]</sup> As Figure 19a illustrates that the proposed structure is made of Au-TiO<sub>2</sub> bi-layer design photoanode fabricating a TiO<sub>2</sub> photonic crystal (PC) layer through a template-assisted sol-gel process on a TiO<sub>2</sub> NR array. By alternating the characteristic pore size of the TiO<sub>2</sub> PC layer, the slow photon region at the red edge of the PC band gap can be proposed to overlap with the strong localized surface plasmon resonance (SPR) region of Au NPs. This phenomenon amplifies the SPR effect and consequently, more hot electrons are generated and injected into the conduction band of TiO<sub>2</sub>. Surface-textured TiO<sub>2</sub> inverse opal nanonetworks,<sup>[128]</sup> N-doped TiO<sub>2</sub> bowl nanoarrays,<sup>[113]</sup> and other novel designs are examples of the proposed structures for PEC performance improvement of a water splitting device. In addition to all of these nanostructures, one of the most frequently used substrates for plasmon induced water splitting is two-dimensional (2D) planar structures. As already mentioned, the generated hot electrons have short diffusion length and can transport for a short distance before they recombine. Moreover, the near field coupling is strong only at the vicinity of the plasmonic metal which is smaller than couple of tens of nanometers. Therefore, the most efficient part of a semiconductor bulk is its surface. Taking all of these factors into consideration, a 2D high mobility plane can efficiently extract these hot carriers and transport them into the contact. As illustrated in Figure 20, employing MoS<sub>2</sub><sup>[104,147]</sup> nanosheets (Figure 20a–b) and CdSe<sup>[112]</sup> nanoplatelets (Figure 20c) are some examples of such designs.

### 3.3. Interface Engineering

Fast hot carriers recombination is the main limiting factor on the substantial improvement in a hot electron driven PEC-WS cell. Therefore, not only the generation of high density of carriers should be satisfied, but also these electrons should be efficiently coupled into transport layer before they get recombined with their conjugate. Therefore, the role of metal-semiconductor interface is significant on the reduction of these carriers recombination.<sup>[148,149]</sup> The utilization of a semiconductor interlayer with a proper band position and band gap not only offers recombination suppression but it can also generate elec-

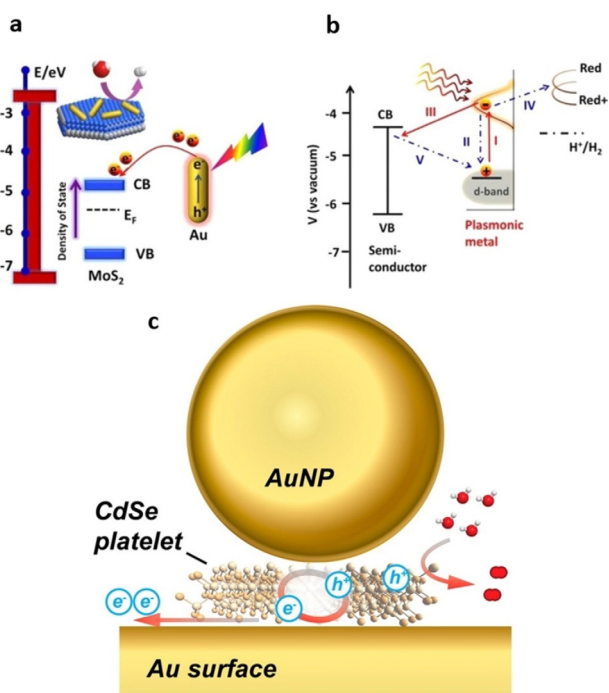


**Figure 20.** a) Coupling of hot electrons to two-dimensional MoS<sub>2</sub> semiconductor design and b) its energy-band diagram.<sup>[147]</sup> c) Schematic representation of electron and hole transfer in AuNP-loaded CdSe nanoplatelets. Reproduced with permission from Ref. [112]. Copyright 2015, American Chemical Society.

tron and hole pairs to boost the photocurrent value of the system. This has been shown in a sandwiched design of ZnO-ZnS-Au where an ultrathin ZnS layer ( $\approx 4$  nm) is uniformly wrapped around the ZnO NR structure<sup>[111]</sup> in a hydrothermal based synthesis approach (as illustrated in Figure 21a). Figure 21b schematically explains the impact of ZnS layer on the PEC performance of the multilayer design. The photoconversion STH efficiency of the design reached to a maximum of 0.21% that was 2-fold and 3.5-fold larger compared to ZnO-Au

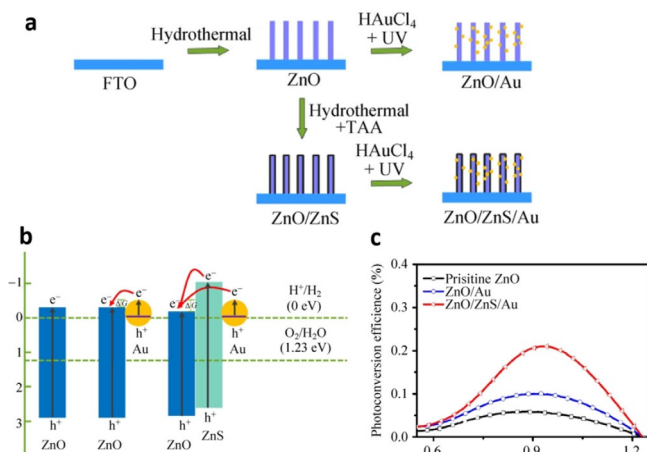


**Figure 21.** The a) preparation route, b) electron transfer dynamics and c) conversion efficiency of a ZnS engineered ZnO-Au plasmonic nanocomposite design. Reproduced with permission from Ref. [111]. Copyright 2015, Springer Nature.

and pristine ZnO photoanodes, respectively. SPR visible light induced hot electrons are injected into ZnS and then they diffuse into ZnO conduction band. However, the location of conduction band of ZnS, which is above that of ZnO, blocks their back reaction and thus carriers' recombination is mitigated. Moreover, under UV irradiation, this ZnS layer gets activated and directly contributes to the photocurrent enhancement of the PEC device. Similar mechanisms have also been found to be responsible for photocurrent enhancement in ZnO (NR)-ZnFe<sub>2</sub>O<sub>4</sub>-Au ternary design.<sup>[125]</sup> However, the difference in this design is the narrow band gap of ZnFe<sub>2</sub>O<sub>4</sub> semiconductor, which makes it active in the visible frequency range (see Figure 22a,b). Therefore, this configuration not only impedes carrier recombination but also it can generate carriers, which in

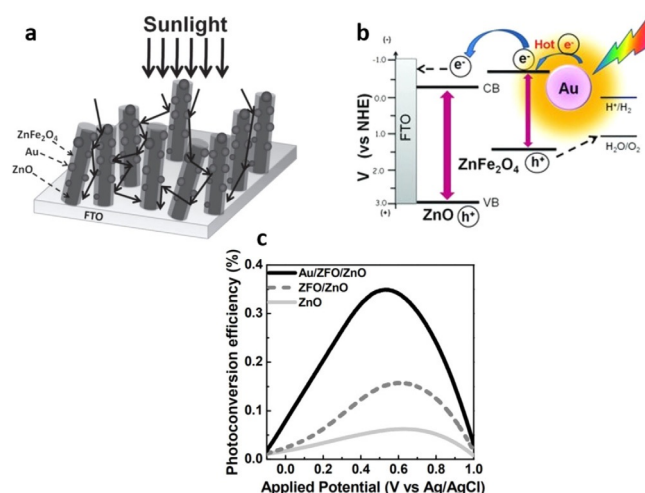


**Figure 22.** The a) structure, b) electron transfer dynamics and c) conversion efficiency of a ZnO-ZnFe<sub>2</sub>O<sub>4</sub>-Au plasmonic hybrid design. Reproduced with permission from Ref. [125]. Copyright 2013, Wiley-VCH.

turn leads to overall photocurrent enhancement. This has been schematically depicted in Figure 22b. As exhibited in Figure 22c, by getting advantage from this property, this design can boost the STH efficiency of the design to a value of about 0.35, which is relatively higher, compared to abovementioned ZnO-ZnS-Au hybrid design. Therefore, utilization of a proper interfacial layer can be envisioned as an alternative approach to substantiate the overall activity of a PEC-WS design. A comparison of the performances (including conditions investigated) of different plasmonic-enhanced photoelectrodes for PEC-WS is presented in Table 1.

## 4. Conclusions and Outlook

Driven by the current growing concern about global climate change and the depletion of fossil fuels, hydrogen (H<sub>2</sub>) is considered to be an attractive energy carrier compared to hydrocarbons since it has the highest gravimetric energy density (140 mJ kg<sup>-1</sup>) and zero carbon emission. Although the production of hydrogen via solar light driven water splitting has a better impact on the environment, the generation of hydrogen is not the only aim for modern photoelectrochemical water

**Table 1.** A comparison on different plasmonic-enhanced photoelectrodes in PEC-WS.

Photoelectrode	Electrolyte, pH	Light Source, Intensity	Efficiency	Year Ref
Au (NP/NR)/ TiO <sub>2</sub> (NW)	1 m NaOH	White-light illumination (AM 1.5G) 100 mW/cm <sup>2</sup>	IPCE ≤ 19% @ UV IPCE ≤ 0.015% @ Vis (at 0 V vs. Ag/AgCl)	2013 [131]
Au (NP)/ ZnFe <sub>2</sub> O <sub>4</sub> / ZnO (NR)	0.1 m Na <sub>2</sub> SO <sub>4</sub>	White-light illumination (AM 1.5G) 100 mW/cm <sup>2</sup>	STH = ≈ 0.35% (at 0.5 V vs. Ag/AgCl)	2013 [125]
Au (NP)/ TiO <sub>2</sub> (inverse opal)	0.24 m Na <sub>2</sub> S and 0.35 m Na <sub>2</sub> SO <sub>3</sub> (pH ≈ 12)	White-light illumination (AM 1.5G) with a 425 nm pass band filter 80 mW/cm <sup>2</sup>	STH = 1% (at ≈ 1 V vs. Ag/AgCl)	2013 [128]
Au (NP)/ TiO <sub>2</sub> (Dendritic NR)	1 m KOH	White-light illumination (AM 1.5G) with a 420 nm pass band filter 100 mW/cm <sup>2</sup>	STH = 1.27% (at 0.64 V vs. RHE)	2013 [106]
Au (nano hole)/ Fe <sub>2</sub> O <sub>3</sub> (NR)	1.0 m NaOH	White-light illumination (AM 1.5G) 100 mW/cm <sup>2</sup>	IPCE = 7.4% @ 425 nm	2013 [145]
Au (NP)/ TiO <sub>2</sub> bilayer (PC-NR)	1 m KOH (pH 13.5)	White-light illumination (AM 1.5G) 100 mW/cm <sup>2</sup>	STH = 0.71% (at 0.64 V vs. RHE)	2014 [150]
Au (NP)/ TiO <sub>2</sub> (NW)	1 m NaOH	λ > 515 nm	Not given	2014 [103]
Au (NP)/ SrTiO <sub>3</sub> (planar)	(HCl)/ (KOH) aqueous solutions	Xe light filtered over the range of 450 nm-850 nm	Not given	2014 [142]
Au (NP)/ TiO <sub>2</sub> (porous film)	1 m NaOH (pH 13)	White-light illumination (AM 1.5G) 100 mW/cm <sup>2</sup>	IPCE = ≈ 2% @ 550 nm	2014 [141]
Au (NP)/ MoS <sub>2</sub> (NS)	0.1 m KH <sub>2</sub> PO <sub>4</sub> (pH 7)	150 W Halogen lamp with a 420 nm pass band filter 350 mW/cm <sup>2</sup>	Not given	2014 [104]
Matchlike Au (NP)/ ZnO (NR)	0.1 m Na <sub>2</sub> SO <sub>4</sub> (pH 7.0)	White-light illumination (AM 1.5G) 100 mW/cm <sup>2</sup>	STH = 0.48% (at 1.05 V vs. RHE)	2014 [146]
Au (NP)/ ZnO (3D Branched NW)	0.5 m Na <sub>2</sub> SO <sub>4</sub> (pH ≈ 7.0)	White-light illumination (AM 1.5G) with a 420 nm pass band filter 100 mW/cm <sup>2</sup>	STH = 0.52% (at ≈ 0.8 V vs. RHE)	2014 [108]
CdS(QDs)/ Au (NP)	0.5 m K <sub>2</sub> SO <sub>4</sub>	White-light illumination (AM 1.5G) with a 420 nm pass band filter	Not given	2014 [138]
Au-Ag (core-shell)/ TiO <sub>2</sub> (NP)	Not given	White-light illumination (AM 1.5G) 100 mW/cm <sup>2</sup>	IPCE ≤ 0.004% @ Vis (at 0 V vs. Ag/AgCl)	2014 [84]
Au (NP)/ ZnO (NPEN)	0.5 m Na <sub>2</sub> SO <sub>4</sub> (pH 6.8)	300 W Xe lamp light source with a 420 nm pass band filter 100 mW/cm <sup>2</sup>	Not given	2015 [105]
Ag (micro flower)/ Si (NW)	0.5 m Na <sub>2</sub> SO <sub>4</sub> (pH 1.0)	White-light illumination (AM 1.5G) 100 mW/cm <sup>2</sup>	IPCE = ≈ 9.1% @ 380 nm IPCE = ≈ 26.3% @ 650 nm (at -1.0 V vs. Ag/AgCl)	2015 [144]
Au (NP)/ ZnO (NR@ nano-platelet)	0.5 m Na <sub>2</sub> SO <sub>4</sub> (pH 6.8)	White-light illumination (AM 1.5G) 100 mW/cm <sup>2</sup>	STH = 0.69% (at 0.42 V vs. Hg/Hg <sub>2</sub> Cl <sub>2</sub> )	2015 [120]
Au (NP)/ ZnS/ ZnO (NR)	0.5 m Na <sub>2</sub> SO <sub>4</sub> (pH ≈ 7.0)	White-light illumination (AM 1.5G) with a 420 nm pass band filter 45 mW/cm <sup>2</sup>	STH = 0.21% (at ≈ 0.928 V vs. RHE)	2015 [111]
Au (NP)/ CdSe (nano platelets)	phosphate buffer (pH 7.0)	200 mw/cm <sup>2</sup> Xe lamp	Not given	2015 [112]
Au (NP)/ TiO <sub>2</sub> (nano bowl)	0.5 m Na <sub>2</sub> SO <sub>4</sub>	White-light illumination (AM 1.5G) 100 mW/cm <sup>2</sup>	Not given	2016 [113]
Au (NP)/ TiO <sub>2</sub> (nano cone)/ AZO	0.1 m Na <sub>2</sub> SO <sub>4</sub> (pH ≈ 6.8)	White-light illumination (AM 1.5G) with a 455 nm pass band filter	STH = 0.73% (at 0.21 V vs. RHE)	2016 [114]
Au (NP)/ RGO/ TiO <sub>2</sub> (NT)	1 m KOH	White-light illumination (AM 1.5G) with a 400 nm pass band filter 100 mW/cm <sup>2</sup>	IPCE = 5.8% @580 nm	2016 [117]
Au (NP)/ TiO <sub>2</sub> (NT)	1 m KOH	White-light illumination (AM 1.5G) with a 400 nm pass band filter 100 mW/cm <sup>2</sup>	STH = 0.81% (at 1.23 V vs. RHE)	2016 [118]
Au (NP)/ TiO <sub>2</sub> (porous film)	0.05 m NaOH	White-light illumination (AM 1.5G) with a 425 nm pass band filter 100 mW/cm <sup>2</sup>	IPCE = 1.27% @ 550 nm	2015 [140]
IrO <sub>x</sub> (NP)/ Au (NP)/ TiO <sub>2</sub> (NR)	0.5 m Na <sub>2</sub> SO <sub>4</sub> (pH ≈ 6)	White-light illumination (AM 1.5G) with a 495 nm pass band filter	IPCE = 0.06% @ 550 nm	2016 [129]

splitting (PEC-WS) systems. Researchers are still tackling some fundamental problems related to the material selection and mechanisms of photosynthetic systems. This Review attempted to scrutinize the concept and technological development toward plasmon-driven PEC-WS, which has been the subject of intensive multidisciplinary research in recent years. The recent strategies based on plasmon-mediated energy transfer are categorized into three classifications as the nanoplasmonic unit (shape, size, composition, and so on), nanostructured support scaffold, and interface engineering. In each section, we highlighted the main function of each strategy and its major impacts on cell performance enhancement. The whole picture of all the strategies serves one ultimate aim, which is to harvest the solar spectrum efficiently in order to enhance photocurrent (up to around  $10 \text{ mA cm}^{-2}$ ) at low or no applied bias. The main figure of merit for a hot-electron-driven water splitting system is, in fact, to maximize the STH efficiency of the cell. The excitation of hot electrons in the metal–semiconductor Schottky junction, if designed properly, can propose several advantages to boost overall absorption:

- 1) Facilitating below band gap absorption by the mediation of electron transfer from the VB to the CB;
- 2) Increasing the inherent absorption capacity of the semiconductor by the excitation of localized surface plasmons in the semiconductor/metal interface using a near-field coupling;
- 3) Reducing electron/hole pair recombination by offering more efficient spatial charge separation due to high electric field amplitudes in the interface;
- 4) Increasing reaction rate of PEC cell through the introduction of proper energetic locations to mediate carriers transfer;
- 5) Providing a high chemical stability due to non-corrosive and non-oxidant nature of noble metals.

For scale-up and long-term usage of plasmonic metal nanostructures combined with semiconductors, high conversion efficiency, high photo (and chemical) stability, and cost-effectiveness are still at the top of the “wanted list”. In light of these demands, several points need to be pursued for further understanding to enhance the light absorption in water splitting system for the future applications;

- 1) Innovations in material architecture for efficient and broad-band light harvesting in which most of the solar spectrum from UV to NIR can be employed for carriers generation. Mixed-metal oxides, perovskites ( $\text{ABO}_3$ ), non-oxide narrow band gap semiconductors, and 2D materials such as graphene and transition metal oxides, combined with earth-abundant metals such as Al and Cu or alloyed noble metals or up-conversion nanocrystals can be used to extend absorption. For substantial performance enhancement, they should also be coupled with optimized performance co-catalysts.
- 2) Plasmonics is a versatile technique to manipulate light in the entire solar spectrum, and considering the ultrafast ki-

netics of hot electron injection, a deep understanding of the kinetics of interfacial electron and hole transfer in photoactive plasmonic materials is necessary. This suggests that hot electrons act as a mediator for the conversion of solar energy to chemical energy.

- 3) To synthesize them with high-throughput, long-term stability and precise control for obtaining different geometries and compositions, defect chemistry, corrosion and surface sciences should be encouraged as well as (photo)electrochemistry. In addition, in the purity and toxicity issues (i.e. metal release), environmental chemistry and green chemistry are also part of this research when it becomes commercial.
- 4) For the best choice of material and nanostructuring, fast theoretical studies and characterization techniques should be conducted and more exploration.
- 5) Newly emerged PEC configurations integrated by photovoltaics and electrolyzers are a big step for water splitting technology toward commercialization. In this case, engineers and materials scientists should be encouraged to work together for designing a highly efficient solar water splitting systems.
- 6) To some extent standardization is necessary to eliminate the efficiency discrepancies stemming from experimental set-ups, conditions, and light sources.

## Acknowledgements

*This work was supported by the Scientific and Technological Research Council of Turkey (TUBITAK), grant number 215Z249. This work is supported by the projects DPT-HAMIT and TUBITAK under Project Nos., 113E331, 114E374, 115F560. One of the authors (E.O.) also acknowledges partial support from the Turkish Academy of Sciences.*

## Conflict of interest

*The authors declare no conflict of interest.*

**Keywords:** artificial photosynthesis • photoelectrochemistry • plasmonics • surface plasmon resonance • water splitting

- [1] C. N. R. Rao, S. R. Lingampalli, *Small* **2016**, *12*, 16.
- [2] L. Meda, L. Abbondanza, *Rev. Adv. Sci. Eng.* **2013**, *2*, 200.
- [3] M. G. Kibria, Z. Mi, *J. Mater. Chem. A* **2016**, *4*, 2801.
- [4] R. Li, *Chin. J. Catal.* **2017**, *38*, 5.
- [5] L. Hammarström, *Faraday Discuss.* **2017**, *198*, 549.
- [6] J. Cen, Q. Wu, M. Liu, A. Orlov, *Green Energy Environ.* **2017**, *2*, 100.
- [7] D. Bae, B. Seger, P. C. K. Vesborg, O. Hansen, I. Chorkendorff, *Chem. Soc. Rev.* **2017**, *46*, 1933.
- [8] C. Jiang, S. J. A. Moniz, A. Wang, T. Zhang, J. Tang, *Chem. Soc. Rev.* **2017**, *46*, 4645.
- [9] Y. Yang, S. Niu, D. Han, T. Liu, G. Wang, Y. Li, *Adv. Energy Mater.* **2017**, *7*, 1700555, 26.
- [10] S. Bai, W. Yin, L. Wang, Z. Li, Y. Xiong, *RSC Adv.* **2016**, *6*, 57446.
- [11] J. Su, L. Vayssieres, *ACS Energy Lett.* **2016**, *1*, 121.
- [12] M. Crespo-Quesada, E. Reisner, *Energy Environ. Sci.* **2017**, *10*, 1116.

- [13] W. T. Qiu, Y. C. Huang, Z. L. Wang, S. Xiao, H. B. Ji, Y. X. Tong, *Acta Phys. Chim. Sin.* **2017**, *33*, 80.
- [14] F. Nandjou, S. Haussener, *J. Phys. D* **2017**, *50*, 124002.
- [15] C. Xiang, A. Z. Weber, S. Ardo, A. Berger, Y. K. Chen, R. Coridan, K. T. Fountaine, S. Haussener, S. Hu, R. Liu, N. S. Lewis, M. A. Modestino, M. M. Shaner, M. R. Singh, J. C. Stevens, K. Sun, K. Walczak, *Angew. Chem. Int. Ed.* **2016**, *55*, 12974; *Angew. Chem.* **2016**, *128*, 13168.
- [16] R. Sathre, J. Greenblatt, K. Walczak, I. D. Sharp, J. C. Stevens, J. W. Ager III, F. A. Houle, *Energy Environ. Sci.* **2016**, *9*, 803.
- [17] A. Fujishima, K. Honda, *Nature* **1972**, *238*, 37.
- [18] M. Barroso, C. a. Mesa, S. R. Pendlebury, A. J. Cowan, T. Hisatomi, K. Sivula, *Proc. Natl. Acad. Sci. USA* **2012**, *109*, 15640.
- [19] C. Xiaobo, S. Shaohua, G. Liejin, M. Samuel, *Chem. Rev.* **2010**, *110*, 6503.
- [20] X. Li, J. Yu, J. Low, Y. Fang, J. Xiao, X. Chen, *J. Mater. Chem. A* **2015**, *3*, 2485.
- [21] K. J. Young, L. A. Martini, R. L. Milot, R. C. Snoeberger, V. S. Batista, C. A. Schmuttenmaer, R. H. Crabtree, G. W. Brudvig, *Coord. Chem. Rev.* **2012**, *256*, 2503.
- [22] S. Bai, L. Wang, Z. Li, Y. Xiong, *Adv. Sci.* **2017**, *4*, 1600216.
- [23] A. G. Tamirat, J. Rick, A. A. Dubale, W.-N. Su, B.-J. Hwang, *Nanoscale Horiz.* **2016**, *1*, 243.
- [24] M. D. Bhatt, J. S. Lee, *J. Mater. Chem. A* **2015**, *3*, 10632.
- [25] T. Singh, T. Lehnen, T. Leuning, S. Mathur, *J. Vac. Sci. Technol. A* **2015**, *33*, 010801.
- [26] L. J. Minggu, W. R. Wan Daud, M. B. Kassim, *Int. J. Hydrogen Energy* **2010**, *35*, 5233.
- [27] X. Li, X. Hao, A. Abudula, G. Guan, *J. Mater. Chem. A* **2016**, *4*, 11973.
- [28] E. Verlage, S. Hu, R. Liu, R. J. R. Jones, K. Sun, C. Xiang, N. S. Lewis, H. A. Atwater, *Energy Environ. Sci.* **2015**, *8*, 3166.
- [29] J. L. Young, M. A. Steiner, H. Döscher, R. M. France, J. A. Turner, T. G. Deutsch, *Nat. Energy* **2017**, *2*, 17028.
- [30] A. Eftekhari, V. J. Babu, S. Ramakrishna, *Int. J. Hydrogen Energy* **2017**, *42*, 11078.
- [31] S. Kumar, K. Ojha, A. K. Ganguli, *Adv. Mater. Interfaces* **2017**, *4*, 1600981.
- [32] S. Bai, J. Jiang, Q. Zhang, Y. Xiong, *Chem. Soc. Rev.* **2015**, *44*, 2893.
- [33] M. A. Modestino, S. M. H. Hashemi, S. Haussener, *Energy Environ. Sci.* **2016**, *9*, 1533.
- [34] S. Pokrant, S. Dilger, S. Landsmann, M. Trottmann, *Mater. Today Energy* **2017**, *5*, 158.
- [35] X. Yang, R. Liu, Y. He, J. Thorne, Z. Zheng, D. Wang, *Nano Res.* **2015**, *8*, 56.
- [36] M. S. Y. Xu, *Am. Mineral.* **2000**, *85*, 543.
- [37] J. Li, N. Wu, *Catal. Sci. Technol.* **2015**, *5*, 1360.
- [38] M. F. Weber, *J. Electrochem. Soc.* **1984**, *131*, 1258.
- [39] M. G. Walter, E. L. Warren, J. R. McKone, S. W. Boettcher, Q. Mi, E. A. Santori, N. S. Lewis, *Chem. Rev.* **2010**, *110*, 6446.
- [40] M. Ge, J. Cai, J. Iocozzia, C. Cao, J. Huang, X. Zhang, J. Shen, S. Wang, S. Zhang, K. Q. Zhang, Y. Lai, Z. Lin, *Int. J. Hydrogen Energy* **2017**, *42*, 8418.
- [41] X. Liu, F. Wang, Q. Wang, *Phys. Chem. Chem. Phys.* **2012**, *14*, 7894.
- [42] Z. Liu, Q. Cai, C. Ma, J. Zhang, J. Liu, *New J. Chem.* **2017**, *41*, 7947.
- [43] K. Tolod, S. Hernández, N. Russo, *Catalysts* **2017**, *7*, 13.
- [44] S. Y. Tee, K. Y. Win, W. S. Teo, L. D. Koh, S. Liu, C. P. Teng, M. Y. Han, *Adv. Sci.* **2017**, *4*, 1600337.
- [45] K. Maeda, K. Domen, *J. Phys. Chem. C* **2007**, *111*, 7851.
- [46] N. M. Gupta, *Renewable Sustainable Energy Rev.* **2017**, *71*, 585.
- [47] R. Abe, M. Higashi, K. Domen, *J. Am. Chem. Soc.* **2010**, *132*, 11828.
- [48] M. Higashi, K. Domen, R. Abe, *J. Am. Chem. Soc.* **2012**, *134*, 6968.
- [49] M. Higashi, K. Domen, R. Abe, *Energy Environ. Sci.* **2011**, *4*, 4138.
- [50] M. Wiegel, M. H. J. Emond, E. R. Stobbe, G. Blasse, *J. Phys. Chem. Solids* **1994**, *55*, 773.
- [51] J. Su, L. Guo, N. Bao, C. A. Grimes, *Nano Lett.* **2011**, *11*, 1928.
- [52] X. Shi, I. Y. Choi, K. Zhang, J. Kwon, D. Y. Kim, J. K. Lee, S. H. Oh, J. K. Kim, J. H. Park, *Nat. Commun.* **2014**, *5*, 4775.
- [53] W. Smith, A. Wolcott, R. C. Fitzmorris, J. Z. Zhang, Y. Zhao, *J. Mater. Chem.* **2011**, *21*, 10792.
- [54] K. Sivula, F. Le Formal, M. Grätzel, *Chem. Mater.* **2009**, *21*, 2862.
- [55] R. Li, Q. Li, L. Zong, X. Wang, J. Yang, *Electrochim. Acta* **2013**, *91*, 30.
- [56] S. Hernández, V. Cauda, A. Chiodoni, S. Dallorto, A. Sacco, D. Hidalgo, E. Celasco, C. F. Pirri, *ACS Appl. Mater. Interfaces* **2014**, *6*, 12153.
- [57] M. Xie, Y. Feng, X. Fu, P. Luan, L. Jing, *J. Alloys Compd.* **2015**, *631*, 120.
- [58] T. Takata, K. Domen, *Dalton Trans.* **2017**, *46*, 10529.
- [59] T. Wang, J. Gong, *Angew. Chem. Int. Ed.* **2015**, *54*, 10718; *Angew. Chem.* **2015**, *127*, 10866.
- [60] J. R. Swierk, T. E. Mallouk, *Chem. Soc. Rev.* **2013**, *42*, 2357.
- [61] M. K. Brennaman, R. J. Dillon, L. Alibabaei, M. K. Gish, C. J. Dares, D. L. Ashford, R. L. House, G. J. Meyer, J. M. Papanikolas, T. J. Meyer, *J. Am. Chem. Soc.* **2016**, *138*, 13085.
- [62] Z. Yu, F. Li, L. Sun, *Energy Environ. Sci.* **2015**, *8*, 760.
- [63] C. C. L. McCrory, S. H. Jung, J. C. Peters, T. F. Jaramillo, *J. Am. Chem. Soc.* **2013**, *135*, 16977.
- [64] C. C. L. McCrory, S. Jung, I. M. Ferrer, S. M. Chatman, J. C. Peters, T. F. Jaramillo, *J. Am. Chem. Soc.* **2015**, *137*, 4347.
- [65] G. Hodes, D. Cahen, J. Manassen, *Nature* **1976**, *260*, 312.
- [66] R. M. May, P. Tapponnier, P. Molnar, *Nature* **1976**, *261*, 402.
- [67] F. P. Koffyberg, F. A. Benko, *J. Electrochem. Soc.* **1981**, *128*, 2476.
- [68] A. Kudo, K. Ueda, H. Kato, I. Mikami, *Catal. Lett.* **1998**, *53*, 229.
- [69] S. U. M. Khan, J. Akikusa, *J. Phys. Chem. B* **1999**, *103*, 7184.
- [70] R. Abe, T. Takata, H. Sugihara, K. Domen, *Chem. Commun.* **2005**, 3829.
- [71] H. A. Atwater, A. Polman, *Nat. Mater.* **2010**, *9*, 865.
- [72] S. A. Maier, H. A. Atwater, *J. Appl. Phys.* **2005**, *98*, 011101.
- [73] I. S. I. Web, S. This, H. Press, N. York, A. Nw, *Science* **2012**, *189*, 189.
- [74] C. Clavero, *Nat. Photonics* **2014**, *8*, 95.
- [75] M. L. Brongersma, N. J. Halas, P. Nordlander, *Nat. Nanotechnol.* **2015**, *10*, 25.
- [76] K. Marchuk, K. A. Willets, *Chem. Phys.* **2014**, *445*, 95.
- [77] Y. H. Jang, Y. J. Jang, S. Kim, L. N. Quan, K. Chung, D. H. Kim, *Chem. Rev.* **2016**, *116*, 14982.
- [78] W. R. Erwin, H. F. Zarick, E. M. Talbert, R. Bardhan, *Energy Environ. Sci.* **2016**, *9*, 1577–1601.
- [79] A. M. Brown, R. Sundararaman, P. Narang, W. A. Goddard, H. A. Atwater, *ACS Nano* **2016**, *10*, 957.
- [80] K. Islam, A. Alnuaimi, E. Battal, A. K. Okyay, A. Nayfeh, *Sol. Energy* **2014**, *103*, 263.
- [81] B. J. Soller, D. G. Hall, *J. Opt. Soc. Am. B* **2002**, *19*, 2437.
- [82] P. K. Jain, K. S. Lee, I. H. El-Sayed, M. A. El-Sayed, *J. Phys. Chem. B* **2006**, *110*, 7238.
- [83] C. S. Kumarasinghe, M. Premaratne, Q. Bao, G. P. Agrawal, *Sci. Rep.* **2015**, *5*, 12140.
- [84] W. R. Erwin, A. Coppola, H. F. Zarick, P. Arora, K. J. Miller, R. Bardhan, *Nanoscale* **2014**, *6*, 12626.
- [85] A. Sousa-Castillo, M. Comesana-Hermo, B. Rodriguez-Gonzalez, M. Perez-Lorenzo, Z. Wang, X. T. Kong, A. O. Govorov, M. A. Correa-Duarte, *J. Phys. Chem. C* **2016**, *120*, 11690.
- [86] G. Baffou, R. Quidant, *Chem. Soc. Rev.* **2014**, *43*, 3898.
- [87] K. Li, M. I. Stockman, D. J. Bergman, *Phys. Rev. Lett.* **2005**, *91*, 227402.
- [88] G. Pellegrini, M. Celebrano, M. Finazzi, P. Biagioni, *J. Phys. Chem. C* **2016**, *120*, 26021.
- [89] J. Sá, G. Tagliabue, P. Friedli, J. Szlachetko, M. H. Rittmann-Frank, F. G. Santomauro, C. J. Milne, H. Sigg, *Energy Environ. Sci.* **2013**, *6*, 3584.
- [90] X. Zhang, Y. L. Chen, R.-S. Liu, D. P. Tsai, *Rep. Prog. Phys.* **2013**, *76*, 046401.
- [91] M. Wang, M. Ye, J. Iocozzia, C. Lin, Z. Lin, *Adv. Sci.* **2015**, *3*, 14.
- [92] R. L. Giesecking, M. A. Ratner, G. C. Schatz, *ACS Symp. Ser.* **2016**, *1245*, Chapter 1, pp. 1–22.
- [93] L. Du, A. Furube, K. Yamamoto, K. Hara, R. Katoh, M. Tachiya, *J. Phys. Chem. C* **2009**, *113*, 6454.
- [94] D. Mongin, E. Shaviv, P. Maioli, A. Crut, U. Banin, N. Del Fatti, F. Vallée, *ACS Nano* **2012**, *6*, 7034.
- [95] T. G. Ulusoy, A. Ghobadi, A. K. Okyay, *J. Mater. Chem. A* **2014**, *2*, 16867.
- [96] A. Ghobadi, H. I. Yavuz, T. G. Ulusoy, K. C. Icli, M. Ozenbas, A. K. Okyay, *Electrochim. Acta* **2015**, *157*, 23.
- [97] A. Ghobadi, T. G. Ulusoy, R. Garifullin, M. O. Guler, A. K. Okyay, *Sci. Rep.* **2016**, *6*, 30587.
- [98] A. K. Chandiran, N. Tetreault, R. Humphry-Baker, F. Kessler, E. Baranoff, C. Yi, M. K. Nazeeruddin, M. Grätzel, *Nano Lett.* **2012**, *12*, 3941.
- [99] C. Prasittichai, J. R. Avila, O. K. Farha, J. T. Hupp, *J. Am. Chem. Soc.* **2013**, *135*, 16328.

- [100] S. K. Cushing, J. Li, F. Meng, T. R. Senty, S. Suri, M. Zhi, M. Li, A. D. Bristow, N. Wu, *J. Am. Chem. Soc.* **2012**, *134*, 15033.
- [101] S. K. Cushing, J. Li, J. Bright, B. T. Yost, P. Zheng, A. D. Bristow, N. Wu, *J. Phys. Chem. C* **2015**, *119*, 16239.
- [102] X. Zhang, Y. Liu, S.-T. Lee, S. Yang, Z. Kang, *Energy Environ. Sci.* **2014**, *7*, 1409.
- [103] J. S. Duchene, B. C. Sweeny, A. C. Johnston-Peck, D. Su, E. A. Stach, W. D. Wei, *Angew. Chem. Int. Ed.* **2014**, *53*, 7887; *Angew. Chem.* **2014**, *126*, 8021.
- [104] Z. Yin, B. Chen, M. Bosman, X. Cao, J. Chen, B. Zheng, H. Zhang, *Small* **2014**, *10*, 3537.
- [105] T. Wang, R. Lv, P. Zhang, C. Li, J. Gong, *Nanoscale* **2015**, *7*, 77.
- [106] F. Su, T. Wang, R. Lv, J. Zhang, P. Zhang, J. Lu, J. Gong, *Nanoscale* **2013**, *5*, 9001.
- [107] J. Zhang, X. Jin, P. I. Morales-Guzman, X. Yu, H. Liu, H. Zhang, L. Razzari, J. P. Claverie, *ACS Nano* **2016**, *10*, 4496.
- [108] X. Zhang, Y. Liu, Z. Kang, *ACS Appl. Mater. Interfaces* **2014**, *6*, 4480.
- [109] S. Mukherjee, F. Libisch, N. Large, O. Neumann, L. V. Brown, J. Cheng, J. B. Lassiter, E. a. Carter, P. Nordlander, N. J. Halas, *Nano Lett.* **2013**, *13*, 240.
- [110] S. Mukherjee, L. Zhou, A. M. Goodman, N. Large, C. Ayala-Orozco, Y. Zhang, P. Nordlander, N. J. Halas, *J. Am. Chem. Soc.* **2014**, *136*, 64.
- [111] Y. Liu, Y. Gu, X. Yan, Z. Kang, S. Lu, Y. Sun, Y. Zhang, *Nano Res.* **2015**, *8*, 2891.
- [112] D. O. Sigle, L. Zhang, S. Ithurria, B. Dubertret, J. J. Baumberg, *J. Phys. Chem. Lett.* **2015**, *6*, 1099.
- [113] X. Wang, R. Long, D. Liu, D. Yang, C. Wang, Y. Xiong, *Nano Energy* **2016**, *24*, 87.
- [114] Y. Mi, L. Wen, R. Xu, Z. Wang, D. Cao, Y. Fang, Y. Lei, *Adv. Energy Mater.* **2016**, *6*, 1501496.
- [115] B. Liu, C.-H. Kuo, J. Chen, Z. Luo, S. Thanneeru, W. Li, W. Song, S. Biswas, S. L. Suib, J. He, *Angew. Chem. Int. Ed.* **2015**, *54*, 9061; *Angew. Chem.* **2015**, *127*, 9189.
- [116] L. Zhang, L. O. Herrmann, J. J. Baumberg, *Sci. Rep.* **2015**, *5*, 12.
- [117] J. Luo, D. Li, Y. Yang, H. Liu, J. Chen, H. Wang, *J. Alloys Compd.* **2016**, *661*, 380.
- [118] J. Luo, J. Chen, H. Wang, H. Liu, *J. Power Sources* **2016**, *303*, 287.
- [119] M. Valenti, D. Dolat, G. Biskos, A. Schmidt-Ott, W. A. Smith, *J. Phys. Chem. C* **2015**, *119*, 2096.
- [120] C. Zhang, M. Shao, F. Ning, S. Xu, Z. Li, M. Wei, D. G. Evans, X. Duan, *Nano Energy* **2015**, *12*, 231.
- [121] H. J. Kim, S. H. Lee, A. A. Upadhye, I. Ro, M. I. Tejedor-tejedor, M. A. Anderson, W. B. Kim, G. W. Huber, *ACS Nano* **2014**, *8*, 10756.
- [122] G. Liu, P. Li, G. Zhao, X. Wang, J. Kong, H. Liu, H. Zhang, K. Chang, X. Meng, T. Kako, J. Ye, *J. Am. Chem. Soc.* **2016**, *138*, 9128.
- [123] K. Qian, B. C. Sweeny, A. C. Johnston-Peck, W. Niu, J. O. Graham, J. S. DuChene, J. Qiu, Y.-C. Wang, M. H. Engelhard, D. Su, E. a. Stach, W. D. Wei, *J. Am. Chem. Soc.* **2014**, *136*, 9842.
- [124] J. Qiu, G. Zeng, P. Pavaskar, Z. Li, S. B. Cronin, *Phys. Chem. Chem. Phys.* **2014**, *16*, 3115.
- [125] A. Sheikh, A. Yengantiwar, M. Deo, S. Kelkar, S. Ogale, *Small* **2013**, *9*, 2091.
- [126] K. Wu, W. E. Rodriguez-Cordoba, Y. Yang, T. Lian, *Nano Lett.* **2013**, *13*, 5255.
- [127] Z. Zhan, J. An, H. Zhang, R. V. Hansen, L. Zheng, *ACS Appl. Mater. Interfaces* **2014**, *6*, 1139.
- [128] K. Kim, P. Thiagarajan, H.-J. Ahn, S.-I. Kim, J.-H. Jang, *Nanoscale* **2013**, *5*, 6254.
- [129] S. F. Hung, F. X. Xiao, Y. Y. Hsu, N. T. Suen, H. Bin Yang, H. M. Chen, B. Liu, *Adv. Energy Mater.* **2016**, *6*, 12.
- [130] G. Liu, T. Wang, W. Zhou, X. Meng, H. Zhang, H. Liu, T. Kako, J. Ye, *J. Mater. Chem. C* **2015**, *3*, 7538.
- [131] Y.-C. Pu, G. Wang, K.-D. Chang, Y. Ling, Y.-K. Lin, B. C. Fitzmorris, C.-M. Liu, X. Lu, Y. Tong, J. Z. Zhang, Y.-J. Hsu, Y. Li, *Nano Lett.* **2013**, *13*, 3817.
- [132] A. Ghobadi, H. Hajian, M. Gokbayrak, S. A. Dereshgi, A. Toprak, B. Butun, E. Ozbay, *Opt. Express* **2017**, *25*, 27624.
- [133] B. Wu, D. Liu, S. Mubeen, T. T. Chuong, M. Moskovits, G. D. Stucky, *J. Am. Chem. Soc.* **2016**, *138*, 1114.
- [134] S. Mubeen, J. Lee, N. Singh, S. Krämer, G. D. Stucky, M. Moskovits, *Nat. Nanotechnol.* **2013**, *8*, 247.
- [135] J. Lee, S. Mubeen, X. Ji, G. D. Stucky, M. Moskovits, *Nano Lett.* **2012**, *12*, 5014.
- [136] A. K. Samal, L. Polavarapu, S. Rodal-Cedeira, L. M. Liz-Marzán, J. Pérez-Juste, I. Pastoriza-Santos, *Langmuir* **2013**, *29*, 15076.
- [137] H. F. Zarick, W. R. Erwin, J. Aufrecht, A. Coppola, B. R. Rogers, C. L. Pint, R. Bardhan, *J. Mater. Chem. A* **2014**, *2*, 7088.
- [138] X. Ma, K. Zhao, H. Tang, Y. Chen, C. Lu, W. Liu, Y. Gao, H. Zhao, Z. Tang, *Small* **2014**, *10*, 4664.
- [139] S. Yu, Y. H. Kim, S. Y. Lee, H. D. Song, J. Yi, *Angew. Chem. Int. Ed.* **2014**, *53*, 11203; *Angew. Chem.* **2014**, *126*, 11385.
- [140] L. J. Brennan, F. Purcell-Milton, A. S. Salmeron, H. Zhang, A. O. Govorov, A. V. Fedorov, Y. K. Gun'ko, *Nanoscale Res. Lett.* **2015**, *10*, 38.
- [141] M. Haro, R. Abargues, I. Herraiz-Cardona, J. Martínez-Pastor, S. Giménez, *Electrochim. Acta* **2014**, *144*, 64.
- [142] Y. Zhong, K. Ueno, Y. Mori, X. Shi, T. Oshikiri, K. Murakoshi, H. Inoue, H. Misawa, *Angew. Chem. Int. Ed.* **2014**, *53*, 10350; *Angew. Chem.* **2014**, *126*, 10518.
- [143] K. Kimura, S. I. Naya, Y. Jin-Nouchi, H. Tada, *J. Phys. Chem. C* **2012**, *116*, 7111.
- [144] C.-J. Chen, M.-G. Chen, C. K. Chen, P. C. Wu, P.-T. Chen, M. Basu, S.-F. Hu, D. P. Tsai, R.-S. Liu, *Chem. Commun.* **2015**, *51*, 549.
- [145] J. Li, S. K. Cushing, P. Zheng, F. Meng, D. Chu, N. Wu, *Nat. Commun.* **2013**, *4*, 2651.
- [146] M. Wu, W. Chen, Y. Shen, F. Huang, C. Li, S. Li, *ACS Appl. Mater. Interfaces* **2014**, *6*, 15052.
- [147] Y. Shi, J. Wang, C. Wang, T. T. Zhai, W. J. Bao, J. J. Xu, X. H. Xia, H. Y. Chen, *J. Am. Chem. Soc.* **2015**, *137*, 7365.
- [148] E. Minutella, F. Schulz, H. Lange, *J. Phys. Chem. Lett.* **2017**, *8*, 4925.
- [149] Y. Nishijima, K. Ueno, Y. Kotake, K. Murakoshi, H. Inoue, H. Misawa, *J. Phys. Chem. Lett.* **2012**, *3*, 1248.
- [150] X. Zhang, Y. Liu, S.-T. Lee, S. Yang, Z. Kang, *Energy Environ. Sci.* **2014**, *7*, 1409.

---

 Manuscript received: September 18, 2017

Revised manuscript received: December 13, 2017

Accepted manuscript online: December 19, 2017

Version of record online: January 11, 2018